



HAL
open science

Gain-of-function IKZF1 variants in humans cause immune dysregulation associated with abnormal T/B cell late differentiation

Akihiro Hoshino, David Boutboul, Yuan Zhang, Hye Sun Kuehn, Jérôme Hadjadj, Nihal Özdemir, Tiraje Celkan, Christoph Walz, Capucine Picard, Christelle Lenoir, et al.

► **To cite this version:**

Akihiro Hoshino, David Boutboul, Yuan Zhang, Hye Sun Kuehn, Jérôme Hadjadj, et al.. Gain-of-function IKZF1 variants in humans cause immune dysregulation associated with abnormal T/B cell late differentiation. *Science Immunology*, 2022, 7 (69), 10.1126/sciimmunol.abi7160 . hal-03864168

HAL Id: hal-03864168

<https://hal.science/hal-03864168>

Submitted on 23 Nov 2022

HAL is a multi-disciplinary open access archive for the deposit and dissemination of scientific research documents, whether they are published or not. The documents may come from teaching and research institutions in France or abroad, or from public or private research centers.

L'archive ouverte pluridisciplinaire **HAL**, est destinée au dépôt et à la diffusion de documents scientifiques de niveau recherche, publiés ou non, émanant des établissements d'enseignement et de recherche français ou étrangers, des laboratoires publics ou privés.

Title: Gain-of-function *IKZF1* variants in humans cause immune dysregulation associated with abnormal T/B-cell late differentiation

Authors: Akihiro Hoshino^{1*}, David Boutboul^{1*}, Yuan Zhang², Hye Sun Kuehn³, Jérôme Hadjadj^{4,5}, Nihal Özdemir⁶, Tiraje Celkan⁷, Christoph Walz⁸, Capucine Picard^{1,5,9}, Christelle Lenoir¹, Nizar Mahlaoui¹⁰, Christoph Klein¹¹, Xiao Peng¹², Antoine Azar¹², Erin Reigh¹³, Morgane Cheminant¹⁴, Alain Fischer^{10,15,16}, Frédéric Rieux-Laucat^{4,5}, Isabelle Callebaut¹⁷, Fabian Hauck^{11†}, Joshua Milner^{2†}, Sergio D. Rosenzweig^{3†} and Sylvain Latour^{*1,5}

Affiliations:

¹Laboratory of Lymphocyte Activation and Susceptibility to EBV infection, INSERM UMR 1163, Imagine Institute, Paris, France;

²Department of Pediatrics, Irving Medical Center, Columbia University, New York, USA;

³Immunology Service, Department of Laboratory Medicine, National Institutes of Health Clinical Center, NIH, USA;

⁴Laboratory of Immunogenetics of Pediatric Autoimmunity, INSERM UMR 1163, Imagine Institute, Paris, France;

⁵Université de Paris, Paris, France;

⁶Kanuni Sultan Süleyman Training and Research Hospital, Pediatric Hematology Oncology Department, Istanbul, Turkey;

⁷Cerrahpasa Medical University, Pediatric Hematology Oncology Department, Istanbul, Turkey;

⁸Institute of Pathology, Faculty of Medicine, Ludwig-Maximilians-Universität München, Munich, Germany;

⁹Study Center for Primary Immunodeficiencies, Necker-Enfants Malades Hospital, APHP, Paris, France;

¹⁰Department of Pediatric Immunology, Hematology and Rheumatology, Necker-Enfants Malades;

¹¹Department of Pediatrics, Dr. von Hauner Children's Hospital, University Hospital, Ludwig-Maximilians-Universität München, Munich, Germany;

¹²Laboratory of Clinical Immunology and Microbiology and the Immune Deficiency Genetics Section, NIH, USA;

¹³Dartmouth-Hitchcock Medical Center, Boston, USA;

¹⁴Department of Adult Hematology, Necker-Enfants Malades Hospital, APHP, Paris, France;

¹⁵Imagine Institute, Paris, France;

¹⁶Collège de France, Paris, France;

¹⁷Sorbonne Université, Muséum National d'Histoire Naturelle, UMR CNRS 7590, Institut de Minéralogie, de Physique des Matériaux et de Cosmochimie, IMPMC, Paris, France

***Corresponding author:** Sylvain Latour, Laboratory of Lymphocyte Activation and Susceptibility to EBV, Equipe Labellisée Ligue Contre le Cancer, Imagine-Inserm UMR 1163, 24 boulevard du Montparnasse, 75015 Paris, France ; Phone : 33 (1) 42 75 43 03 ; FAX : 33 (1) 75 42 21 ; e-mail : sylvain.latour@inserm.fr; ORCID : 0000-0001-8238-4391

† Equal contribution

Abstract: IKZF1/IKAROS is a key transcription factor of lymphocyte development expressed throughout hematopoiesis. Heterozygous germline *IKZF1* haplo-insufficient (*IKZF1*^{HI}) and dominant negative (*IKZF1*^{DN}) variants in humans cause B-cell immune deficiency and combined immunodeficiency. Herein, we identified new heterozygous *IKZF1* variants (R183C/H) located in the DNA binding domain in 8 individuals with inflammatory, autoimmune, allergic symptoms and abnormal plasma-cell (PC) proliferation. Leukocytes of patients exhibited specific defects including impaired IL-2 production by T cells, T helper (Th) skewing toward Th2, low numbers of regulatory T cells (Treg), eosinophilia and abnormal PC proliferation. In contrast to *IKZF1*^{HI} and *IKZF1*^{DN}, *IKZF1*^{R183H/C} proteins showed increased DNA binding associated with increased gene expression of Th2 and PC differentiation, thus demonstrating that *IKZF1*^{R183H/C} behave as gain-of-function (GOF) alleles. In vitro, lenalidomide, known to degrade IKZF1 corrected Th2 and PC abnormalities caused by *IKZF1*^{R183H/C}. These data extend the spectrum of pathological mechanisms associated with *IKZF1* deficiencies and highlight the role of IKZF1 in late lymphoid differentiation stages.

One Sentence Summary: Immune dysregulation caused by *IKZF1* gain-of-function variants

Main Text:

INTRODUCTION

IKAROS encoded by *IKZF1* is a master transcription factor of lymphocyte development and hematopoiesis and has the role of a tumor suppressor gene (1, 2). IKZF1/IKAROS contains a DNA-binding domain consisting of 4 Zinc fingers (ZFs). It is mainly involved in repression of gene expression through binding to DNA at the pericentromeric heterochromatin (PC-HC) regions and by interacting with the polycomb repressive and the nucleosome remodeling and deacetylase complexes (2). Studies in mouse have revealed that Ikaros has critical roles at many stages of hematopoiesis likely through its ability to interact and regulate hundreds of genes having the core consensus sequence GGGAA in their promoter (3). Several mouse models of Ikaros/Ikzf1 deficiency including mice carrying null (*Ikzf1^{null}*), DN (*Ikzf1^{DN}*) and missense (*Ikzf1^{H191R}*) variants have been reported with different abnormalities and severity affecting the hematopoiesis of lymphoid, myeloid and/or erythroid lineages including occurrence of malignant lymphoproliferations (1, 4, 5). In humans, somatic and constitutive LOF or HI genetic alterations in *IKZF1* are associated with a high risk of leukemia (6, 7). Recently, we and others identified immunodeficient patients carrying heterozygous germline HI or DN variants in *IKZF1*, hereafter denoted as *IKZF1^{HI}* and *IKZF1^{DN}* respectively (8–10). Patients with *IKZF1^{HI}* are characterized by progressive B-cell deficiency, autoimmune disease (in ~20%) and B-cell precursor acute lymphoblastic leukemia (BCP-ALL) (in ~10%). Patients with *IKZF1^{DN}* develop more severe and early-onset manifestations consisting B, T and myeloid cell defects, abnormal erythroid hematopoiesis and occurrence of T-cell ALL (in ~10%). All patients had severe bacterial and viral infections including pneumonia with *Pneumocystis jirovecii*. More recently, variants causing haploinsufficiency of the dimerization domain (denoted *IKZF1^{DD}*) have been reported in patients with hematocytopenia and malignancies (11). In the present study, we report new germline heterozygous genetic variants in *IKZF1* that behave functionally as gain-of-function (GOF) causing a novel disease entity mostly characterized by immune dysregulation symptoms. Our results show that tight regulation of IKZF1 is required for Th, Treg and PC differentiation.

RESULTS

Identification of novel heterozygous variants in *IKZF1*

Whole-exome sequencing (WES) was performed in four unrelated families presenting with multiple autoimmune, allergic and lymphoproliferative manifestations and infections, including two with apparent autosomal dominant inheritance (Fig. 1A and Table 1). Of note, patient A1 was previously reported in a large cohort of patients with Evans syndrome (12). Lymphoproliferative disease was noticed in four patients (from three families) corresponding to polyclonal plasma cell (PC) proliferation. Histopathological analysis of lymph nodes from B1 and her daughter (B2) indicated Rosai-Dorfman disease and follicular hyperplasia, respectively, with the remarkable infiltration of the PCs expressing IgG4 (Fig. 1B). Extensive IgG4+ PC infiltration with elevated serum IgG4 levels was also confirmed in lymph nodes, intestine and bile duct from C1, meeting the diagnosis of IgG4-related disease (table S1). Polyclonal PC proliferation was observed in the bone marrow from D1 (data not shown). WES identified two heterozygous *IKZF1* missense variants g.7:50382665C>T (c.548G>A, p.R183H) and g.7:50382666G>A (c.547C>T, p.R183C) in families A, B and C and family D, respectively. In family A and C, the variant was not present in the parents, suggesting de novo occurrences of the variant in the patients. R183H/C variants are

not reported in the gnomAD, ExAC, 1000 Genomes Project databases and the exome data base of our Institute (17,325 exomes). No other variants were found in genes associated with immunodeficiency or immune dysregulation (data not shown). The variant was also identified in the asymptomatic 16 years old individual B3. He remains without symptoms possibly because of his young age or incomplete penetrance as it was observed in individuals with *IKZF1*^{HI} or *IKZF1*^{DD} variants (8, 9, 11). Interestingly, clinical phenotypes associated with R183H/C variants appeared to differ from those associated with previously described *IKZF1*^{HI}, *IKZF1*^{DN} or *IKZF1*^{DD} variants, thus suggesting that *IKZF1*^{R183H/C} variants behave differently (Fig. 1C). Various autoantibodies were detectable in several *IKZF1*^{GOF} patients (Table 1). Four out five patients tested exhibited abnormally elevated IgE levels (table S2). Notably, atopic and allergic diseases as well as PC proliferation and infiltration have not been reported in patients with *IKZF1*^{HI}, *IKZF1*^{DN} or *IKZF1*^{DD} variants (n > 70) (8–11).

IKZF1^{HI} and *IKZF1*^{DN} variants have been associated with abrogated DNA-binding activity and/or foci formation (8–10), while *IKZF1*^{DD} variants impair dimerization, protein stability and post-translational modifications (11). *IKZF1*^{HI} and *IKZF1*^{DN} variants are located within the DNA-binding domain, the ZFs1-4, and affect critical amino acids for interaction with DNA bases, coordination of zinc atom or maintenance of the finger structure (13). The residue R183 located within the ZF3 at position -8 relative to first zinc-coordinating histidine is highly conserved among species (Fig. 1D and fig. S1A). Residues -1, -4 and -7, lying on the protein-DNA interface are involved in H-bonds with DNA bases in the major groove (14). According to known 3D structures of ZF arrays containing an arginine at the -8 position (fig. S1B), R183 likely interacts with DNA phosphate through a salt-bridge, rather than directly with DNA bases as residues -1, -4 and -7, especially because -7 is already occupied by an arginine, as in the mouse Znf568 ZF7. In addition, H-bonds are also likely to occur between the side chain N atoms of R183 and the main chain oxygen atom of amino acids within the linker joining the ZF3 to the preceding ZF2, as observed for the ZF10 and ZF12 of PRDM9 (Fig. 1E and fig. S1C) (15). Hence, R183 seems to be critical to restrict the flexibility of the ZF3 and replacement to C or H (or any other amino acid) may thus release this constraint and improve the adaptability and the global affinity of the ZF3. Taken together, therefore, these observations prompted us to examine the possibility that the R183H/C variants behave differently than previously reported *IKZF1* variants, causing a novel immune dysregulation associated with inflammation, autoimmunity, and allergy symptoms and PC proliferation.

Increased DNA binding and gene regulation of *IKZF1*^{R183H/C} variants

R183H/C variants (*IKZF1*^{R183H/C}) were first evaluated in transient expression experiments in HEK-293T and NIH-3T3 cells (8–10). Both *IKZF1*^{R183H} and *IKZF1*^{R183C} had similar protein expression levels in the nuclear fraction to those of the wild-type *IKZF1* (*IKZF1*^{WT}) and two variants *IKZF1*^{R162Q} and *IKZF1*^{N159S} known as haploinsufficient (*IKZF1*^{HI}) (8, 9) and dominant-negative (*IKZF1*^{DN}) (10) variants, respectively (Fig. 2A). Confocal microscopy analysis showed that *IKZF1*^{R183H/C} like *IKZF1*^{WT} exhibited nuclear punctate staining pattern with foci (Fig. 2B), whereas *IKZF1*^{N159S} and *IKZF1*^{R162Q} displayed abnormal diffuse nuclear localization as previously described (8–10). Similar results were obtained by analyzing T cells from A1 and B2 that were activated with anti-CD3/CD28-coated beads (fig. S2A). When co-expressed with *IKZF1*^{WT}, *IKZF1*^{R183H/C} mutants dimerized and formed multi-protein complexes similarly as *IKZF1*^{N159S} and *IKZF1*^{R162Q} (fig. S2B). These findings indicate that R183H/C variants did neither result in abnormal *IKZF1* protein expression nor nuclear localization. Next, we directly assessed their

DNA-binding capacity by electrophoretic mobility shift assays (EMSA) performed with the IK-bs4 and γ -Sat8 DNA consensus probes for IKZF1 specific of PC-HC (Fig. 2, C and D). Like IKZF1^{WT}, IKZF1^{R183H/C} were able to bind to the probes, whereas IKZF1^{N159S} and IKZF1^{R162Q} were not. However, significantly more intense shifts (more than three-fold of magnitude) were obtained with IKZF1^{R183H/C} than with IKZF1^{WT} suggesting that IKZF1^{R183H/C} had enhanced binding to DNA. Consistent with this increased binding to DNA, IKZF1^{R183H/C} expression resulted in hyper-repression of the *HES1* and *MCL1* promoter activities and the hyper-activation of the *MSH2* promoter activity (when compared to IKZF1^{WT}), which are known targets of IKZF1 (Fig. 2E) (16, 17). In contrast, expression of IKZF1^{N159S} and IKZF1^{R162Q} had no effect as expected for loss-of-function variants. These data show that the properties of the R183H/C variants differ from that previously ascribed to HI and DN variants suggesting that IKZF1^{R183H/C} behave as GOF variants (hereafter also denoted IKZF1^{GOF}).

Abnormal lymphopoiesis and hematopoiesis in patients with *IKZF1*^{R183H/C} variants

In vivo consequences of *IKZF1*^{GOF} were further evaluated by analysis of peripheral blood subsets in patients and compared to those of *IKZF1*^{HI} and *IKZF1*^{DN} patients. *Ikzf1*^{null} mice and both *IKZF1*^{HI} and *IKZF1*^{DN} patients showed early B-cell developmental arrest leading to significantly decreased B cells and hypogammaglobunemia (1, 8–10). In contrast, *IKZF1*^{GOF} patients showed normal or slightly decreased B-cell counts associated with normal or elevated serum immunoglobulin levels (Fig. 3A and table S2). However, all patients had low proportions of plasmablasts (fig. S3A). Analysis of T lymphocytes showed a strong increase of CD4/CD8 ratio in two *IKZF1*^{GOF} patients, consistent with the limitation of autocrine IL-2 production by *Ikzf1* shown in mouse CD8⁺ T cells (fig. S3B) (18). Furthermore, T cells were strongly skewed to terminally differentiated memory phenotypes with increased proportions of CD4⁺ effector memory, CD8⁺CD57⁺ senescent and exhausted T cells (CD8⁺ T_{EMRA}) (Fig. 3A and fig. S3B). NK cell and eosinophil counts as well as hemoglobin levels were elevated, while NK cells and mDCs were in the normal ranges. These parameters displayed the opposite pattern in *IKZF1*^{HI} and *IKZF1*^{DN} patients (Fig. 3A and fig. S3C). Of note, the asymptomatic individual B3 also showed immunological and hematological abnormalities. Altogether, these observations are suggestive of perturbed lymphopoiesis and hematopoiesis in *IKZF1*^{GOF} patients, but differently than in patients with *IKZF1*^{DN} or *IKZF1*^{HI} and consistent with a hyperactivity of the *IKZF1*^{GOF} proteins. They are also in favor of a role of *IKZF1* in late T/B-cell differentiation.

Impaired IL-2 production and Th1/Th2 unbalance with *IKZF1*^{R183H/C} variants

Functions of T cells from *IKZF1*^{GOF} (*IKZF1*^{R183H/C}) patients were further analyzed and compared with T cells of patients with *IKZF1*^{HI} (*IKZF1*^{R143W}) (19) and *IKZF1*^{DN} (*IKZF1*^{N159T}) (10) variants. First, *IKZF1*^{R183H}-expressing T cells showed comparable proliferation in response to CD3 stimulation despite a high frequency of terminally differentiated effector memory T cells in several patients (fig. S4, A and B), which are known to have a decreased capacity to proliferate (20). In contrast, *IKZF1*^{N159T}-expressing T cells exhibited decreased proliferation as previously reported (10). We next evaluated whether *IKZF1*^{GOF} could influence IL-2 production and Th1/2 differentiation since murine *Ikzf1* was shown to repress *Il2* and *Tbx21/T-bet* gene expression (21–23). CD4⁺ T-cell blasts of *IKZF1*^{GOF} patients exhibited a marked decrease of IL-2 production after phorbol myristate acetate (PMA) and ionomycin stimulation when compared to control *IKZF1*^{WT} T cells (Fig. 3, B and D). In contrast, *IKZF1*^{HI} and *IKZF1*^{DN} patients showed increased IL-2

production, that was even more pronounced in *IKZF1*^{DN} T cells. We also analyzed production of IFN- γ and IL-4 by activated CD4⁺ T cells (Fig. 3, C and D). *IKZF1*^{GOF} CD4⁺ T-cell blasts displayed decreased IFN- γ and increased IL-4 expression when compared to *IKZF1*^{WT}, *IKZF1*^{HI} and *IKZF1*^{DN} cells. As previously reported, both IFN- γ and IL-4 were less expressed in *IKZF1*^{DN} CD4⁺ T cells, likely due to the strong reduction of memory T cells and impaired T-cell memory differentiation that is associated with *IKZF1*^{DN} variants (10). Similar decreased IFN- γ and increased IL-4 production were also observed with fresh *IKZF1*^{R183C}-expressing CD4⁺ T cells (fig. S4C). To better characterize these abnormalities in Th1/Th2 differentiation, we examined the expression of the master transcription regulators *TBX21/T-bet*, and *GATA3* and *MAF* involved in Th1 and Th2 lineage commitments, respectively (Fig. 3E). mRNA expression levels of *TBX21/T-bet* were found to be increased in purified CD4⁺ T-cell blasts from *IKZF1*^{HI} and *IKZF1*^{DN} patients and decreased from *IKZF1*^{GOF} patients. Conversely, higher *GATA3* and *MAF* mRNA levels were observed in *IKZF1*^{GOF} CD4 T cells. These results were consistent with the results of cytokine productions and murine studies.

To further demonstrate the effect of the *IKZF1* variants in IL-2 production and Th1/Th2 differentiation, purified CD4⁺ naïve T cells from healthy controls were infected with lentiviral vector-encoding *IKZF1*^{R183H}, *IKZF1*^{R183C}, *IKZF1*^{R162Q} (*IKZF1*^{HI}), *IKZF1*^{N159S} (*IKZF1*^{DN}), *IKZF1*^{WT} or an empty vector. Cells expressing similar levels of the different variants were then cultured with anti-CD3 mAb-coated plates for 7 days, and IL-2, IL-4, IFN- γ and *TBX21/T-bet* expression was measured after stimulation with PMA and ionomycin (Fig. 4A). *IKZF1*^{HI} and *IKZF1*^{DN} induced the highest proportion of cells expressing IL-2 and IFN- γ (Fig. 4B), and the highest levels of *TBX21/T-bet* mRNA (Fig. 4C). On the other hand, IL-4 expression was significantly increased by *IKZF1*^{R183C} and *IKZF1*^{R183H}, whereas these variants significantly reduced IL-2 and IFN- γ expression and *TBX21/T-bet* levels. As expected, lenalidomide that causes the degradation of *IKZF1*, increased the proportion of IL-2 and IFN- γ positive cells and decreased IL-4 positive cells to a similar extent with all *IKZF1* variants and wild-type *IKZF1*. Therefore, these results indicate that expression of *IKZF1*^{R183H/C} results in a strong skewing towards Th2 differentiation in contrast to the other *IKZF1*^{HI} and *IKZF1*^{DN} variants.

Impaired Treg differentiation with *IKZF1*^{R183H/C} variants

IL-2 plays an important role in the development, long-term survival and suppressor function of Treg, while follicular helper T cell (Tfh) differentiation can be negatively regulated by IL-2 signaling (24, 25). Because IL-2 production was impaired in *IKZF1*^{GOF} expressing T cells, we evaluated Treg and Tfh in *IKZF1*^{GOF} patients that were compared with *IKZF1*^{HI} and *IKZF1*^{DN} patients. CD4⁺FOXP3⁺ T cells are divided in three subpopulations: CD45RA⁺FOXP3^{low}, CD45RA⁻FOXP3^{high} and CD45RA⁻FOXP3^{low} corresponding to naïve Treg, effector Treg and non-Treg/follicular regulatory T cells (Tfr), respectively (26) (Fig. 5A). The patient with *IKZF1*^{HI} (*IKZF1*^{R143W}) showed normal CD4⁺FOXP3⁺ frequency with comparable fractions, whereas effector Treg and non-Treg/Tfr frequency was reduced in the *IKZF1*^{DN} (*IKZF1*^{N159T}) patient, likely due to reduction of CD45RA⁻ T cells as previously shown (10). However, in *IKZF1*^{GOF} patients, the frequency of CD4⁺FOXP3⁺ cells were markedly decreased, and effector Treg were virtually absent. Consistent with a central role of defective IL-2 production in the decrease of Treg in *IKZF1*^{GOF} patients, Treg normally differentiated in presence of IL-2 from CD4⁺ naïve T cells from patient A1 (Fig. 5B). While circulating Tfh frequencies corresponding to CD4⁺CD45RA⁻CXCR5⁺ T cells were decreased in *IKZF1*^{HI} and *IKZF1*^{DN} patients, A1 and B2 exhibited significantly increased Tfh (Fig. 5C). However, among them circulating CD45RA⁻FOXP3⁺ Tfr were

comparable in each patient. Therefore, these results suggest that in $IKZF1^{GOF}$ patients Treg differentiation is compromised as the result of impaired IL-2 production.

Abnormal plasma-cell differentiation with $IKZF1^{R183H/C}$ variants

Lastly, we examined the effect of $IKZF1^{GOF}$ on PC differentiation as half of the patients exhibited abnormal PC proliferation and accumulation in tissues. Although a direct role of $IKZF1$ on PC differentiation has not been described, lenalidomide was shown to inhibit the generation of PCs in association with decreased IRF4 expression (27). We analyzed B-cell differentiation into pre-plasmablasts, plasmablasts and PCs from purified circulating memory B cells of the patients with $IKZF1^{GOF}$. In patients with $IKZF1^{HI}$ or $IKZF1^{DN}$, circulating memory B cells were too scarce to assess their differentiation. Counts of PCs differentiated from memory B cells of $IKZF1^{GOF}$ patients were significantly higher than those from $IKZF1^{WT}$ memory B cells (Fig. 6, A and B) and correlated with increased expression of IRF4 (Fig. 6C). Since IRF4 is a known target of $IKZF1$ in human and has an important role in PC differentiation (28, 29), these findings suggest that $IKZF1^{GOF}$ enhanced PC differentiation and proliferation through at least IRF4 deregulation.

The fact that patients expressing $IKZF1^{R183C/H}$ developed abnormal PC proliferation might suggest a role of $IKZF1$ in multiple myeloma (MM). To explore this possibility, we reviewed $IKZF1$ somatic variants in public and published available genetic data banks of BCP-ALL and MM. Data from several cohorts of a total 2,959 patients with BCP-ALL including Philadelphia-positive BCP-ALL and several cohorts of a total 1,838 patients with MM were analyzed (30–33) (Fig. 6D). We observed significantly increased frequencies of $IKZF1$ variants in BCP-ALL (3.1%, 91/2,959) compared with MM (0.4%, 8/1,838) ($P = 4.0 \times 10^{-10}$) (Fig. 6E and table S3). Among those, 34 variants found in BCP-ALL were nonsense or frameshift variants, whereas none of these were identified in MM. Of note, several variants (C150R, N159S, R162W and H167R), described in patients with $IKZF1^{HI}$ or $IKZF1^{DN}$ (8, 9, 19), were found in BCP-ALL. Importantly, the R183C variant was only found in MM, highlighting its role in PC proliferation. These findings are consistent with the fact that $IKZF1$ acts as a tumor suppressor of BCP-ALL, while $IKZF1$ -IRF4-c-Myc axis is involved in PC proliferation and MM (34).

DISCUSSION

We herein report 8 individuals harboring heterozygous $IKZF1^{R183H}$ or $IKZF1^{R183C}$ variants associated with GOF effects. The clinical phenotypes and pathophysiology associated with $IKZF1^{R183H/C}$ differ from those of previously reported patients with $IKZF1^{HI}$, $IKZF1^{DN}$ and $IKZF1^{DD}$ and should therefore be considered as a novel IKAROS-associated disease entity. This novel condition is characterized by immune dysregulation manifestations including inflammation, autoimmunity, atopy and polyclonal PC proliferation.

Our identification of $IKZF1^{GOF}$ variants highlights the involvement of $IKZF1$ at the later stage of lymphoid development, Th1/2 differentiation and PC differentiation (Fig. S5). We showed that $IKZF1^{GOF}$ are associated with decreased Th1 and increased Th2 differentiation, while $IKZF1^{HI}$ exhibit the opposite pattern and $IKZF1^{DN}$ is associated with overall defective Th differentiation. Since $Ikzf1^{null}$ mice display reduced numbers of thymocytes and no B cells, prior studies mainly focused on the role of $Ikzf1$ in early lymphopoiesis and lymphocyte development stages (2). However, recent studies have also suggested a role of $Ikzf1$ at later stages of lymphocyte differentiation (21, 22, 35). In particular, one study showed that absence of $Ikzf1$ resulted in impaired Th2 differentiation associated with defective repression of $Tbx21$ expression and

activation of *Maf* and *Gata3* expression (21) consistent with our observations in humans with *IKZF1*^{HI} and *IKZF1*^{DN}. In addition to the direct binding of *Ikzf1* to the *Tbx21* promoter (22), regulation of *Ifng* or *Il2* expression by *Ikzf1* likely participates to the repression of Th1 differentiation, thus contributing to Th2 differentiation (36). In agreement with this study, Th2 polarizing conditions resulted in increased IFN- γ expression in a conditional *Ikzf1* knockout mouse model (35). Conversely, we showed that *IKZF1*^{R183C/H} (*IKZF1*^{GOF}) (in patients or when ectopically expressed in normal T cells) led to reduced IL-2, IFN- γ and *TBX21* and increased IL-4, *GATA3*, *MAF* expression. Thus, our observations in human are fully concordant with mice studies. Together, both support a direct role of *IKZF1* in Th differentiation through repression and activation of Th1 and Th2 differentiation programs, respectively. Conjunction of increased Th2 differentiation with increased eosinophils, Tfh and/or hyper IgE very likely contributes to the development of allergic manifestations in the patients.

The observations of PC proliferation in 4/8 (50%) patients with *IKZF1*^{R183H/C} suggest that *IKZF1* is directly involved in PC differentiation and/or maintenance, likely through the increased expression of IRF4, although other genes related to PC differentiation such as *Blimp-1/PRDM1* or *BCL6* might be involved. In *Ikzf1*^{null} mice, the severe block of early B-cell development did not allow the evaluation of *Ikzf1* in PC differentiation. However, there is some indirect evidence of *IKZF1* involvement in PC proliferation and differentiation in human. *IKZF1/IKZF3* (AIOLOS)-IRF4-c-Myc axis has been found to be essential for MM cells (34), and lenalidomide, which causes the degradation of *IKZF1/IKZF3*, is used to treat patients with MM (28, 29). A previous report showed that long-term lenalidomide treatment did not affect PC counts supporting a role of *IKZF1* in PC differentiation rather than the survival or maintenance of PCs (27). Importantly, by reviewing *IKZF1* somatic variants in patients with MM, we identified several MM with heterozygous variants in *IKZF1* including one *IKZF1*^{R183C}, data consistent with its critical role in PC proliferation and differentiation. However, none of the patients with germline *IKZF1*^{R183H/C} have developed MM until now. Additional genetic somatic events may be required to transform benign PC proliferation to MM. Interestingly, most of PCs obtained by biopsies expressed IgG4, clinically consistent with IgG4-related disease. Furthermore, although we could evaluate in only 1 patient, antibodies to *Streptococcus pneumoniae*, of which IgG2 was the most effective subclass, were absent that could suggest IgG2 class-switch impairment for the benefit of IgG4. Immunoglobulin class switching is controlled by specific cytokines, among which the Th2 cytokine, IL-4 has a central role in IgG4 and IgE class switching (37). Thus, Th skewing towards Th2 by *IKZF1*^{GOF} likely participates to increased PC IgG4+ and enhanced IgG4 and IgE in patients.

Interestingly, both *IKZF1*^{HI}, *IKZF1*^{DD} and *IKZF1*^{GOF} variants are associated with autoimmune diseases although they have opposite functional consequences. In patients with *IKZF1*^{HI}, autoimmune diseases include cytopenia, systemic lupus erythematosus (SLE), antiphospholipid syndrome and myasthenia gravis (9, 38, 39), in those with *IKZF1*^{DD}, autoimmune hemolytic anemia and thrombocytopenia were prevalent. With the exception of cytopenia, patients with *IKZF1*^{GOF} developed different autoimmune diseases including type 1 diabetes mellitus, enteritis, autoimmune hepatitis, Hashimoto thyroiditis, leucocytoclastic vasculitis, vitiligo, and alopecia. Furthermore, in contrast to *IKZF1*^{HI} patients and *IKZF1*^{DD} who mostly had a single organ autoimmune manifestation, *IKZF1*^{GOF} patients often developed multiple autoimmune diseases. Given their distinct functional consequences, autoimmunity associated with *IKZF1*^{HI} and *IKZF1*^{DD} vs. *IKZF1*^{GOF} may result from different mechanisms, that are associated with inflammatory symptoms such as colitis in several patients. In autoimmunity associated with *IKZF1*^{HI}, the

following evidences suggest a central role of B cells : i) *IKZF1*^{HI} and *IKZF1*^{DD} patients are mostly characterized by B-cell defects, while T cells are not or minimally affected ii) although *IKZF1*^{HI} and *IKZF1*^{DD} patients developed progressive hypogammaglobulinemia with B-cell deficiency, most of them did not yet exhibit severe hypogammaglobulinemia at the onset of the autoimmune manifestations (9, 38, 39) iii) autoimmune symptoms are ameliorated after development of hypogammaglobulinemia in several *IKZF1*^{HI} and *IKZF1*^{DD} patients (9, 10) and are successfully treated by the depletion of B cells with rituximab (40). Finally, in mouse *Ikzf1* prevents autoimmunity by controlling anergy and Toll-like receptor signaling in B cells (41). In contrast, autoimmune diseases in *IKZF1*^{GOF} patients may rather involve T lymphocytes as patients exhibited a profound defect in Treg, while Treg are normal in patients with *IKZF1*^{HI}. In support to this hypothesis, autoimmune diseases associated with *IKZF1*^{GOF} share similar clinical features with those found in inborn errors of immunity associated impaired Treg such as IPEX syndrome and CTLA4 haploinsufficiency (42). *IKZF1*^{GOF} caused hyper-repression of IL-2, which may contribute to the decreased numbers of Treg and thereby autoimmunity in patients. Decreased Treg associated with various autoimmune diseases are indeed also observed in patients with impaired IL-2 signaling, such as IL-2R β deficiency, CD25 deficiency and STAT5b deficiency (42).

Interestingly, *IKZF1*-degrading immunomodulatory drugs such as lenalidomide that is currently used in the treatment of MM (28, 29) may be a suitable therapeutic option to treat PC proliferations, autoimmune and allergic symptoms in patients with *IKZF1*^{GOF}, as we showed that addition of lenalidomide in vitro blocked abnormal functions of *IKZF1*^{GOF} variants.

MATERIALS AND METHODS

Study design

The objective of this study was to characterize molecularly and functionally new genetic variants in *IKZF1* found by whole exome sequencing in 8 patients and to provide evidence that these variants are causal of their disease. The effect of these new *IKZF1* mutants was compared to previous reported variants, including comparison with samples of patients carrying these previously reported variants. Blood aged samples from healthy individuals were used as controls. All clinical data have reviewed independently at least by two physicians including one involved in the follow-up of the patient. Recombinant *IKZF1* proteins produced in HEK-293T were used to determine the consequences of the mutations on protein expression, nuclear localization, binding to DNA by EMSA and promoter activity using luciferase reporter gene assays. Functional assays in cells include analysis of gene expression by qPCR, cytokines production, proliferation and membrane markers analyzed by flow cytometry. Assays were performed with cells of patients. and some findings were confirmed in normal cells in which *IKZF1* mutants were ectopically expressed using lentiviral vectors. Our study also includes the review of whole exome sequencing public data bases for *IKZF1* variants. All data presented are representative of data collected during this study. Experimental replication and identification of patients tested are indicated in the figures and legends.

Study approval and human samples

This study was conducted in accordance with the Helsinki Declaration and local legislation and ethical guidelines and has been approved by the France II Comité de Protection des Personnes de l'Île de la French advisory committee. Informed consent was obtained from patients or their parents. Blood from health donors was obtained under approved protocols. Patients with *IKZF1*^{HI} (R162Q, R162W, C147R) and *IKZF1*^{DN} (N159S, N159T) variants for which blood samples have

been used in this study have been described elsewhere^{16,17}, excepted for the patient carrier of *IKZF1*^{R143W} that was identified in our hospital.

Genetic analysis and bioinformatics

WES and data analysis were performed in the probands and their parents from genomic DNA from whole blood. Exome capture was carried out with an exome enrichment kit (TruSeq; Illumina), and massively parallel sequencing was performed with a HiSeq2500 sequencing system (Illumina) with 100-bp paired-end reads. Data were processed with an in-house-constructed analysis pipeline, which aligned the reads by using the BWA31, counted variant allele numbers by using SAMtools, and annotated genes by using ANNOVAR33. Sanger sequencing was performed to validate the results. Other family members were tested by Sanger sequencing.

Cell culture and expansion of T-cell blasts

Ficoll-isolated PBMCs were cultured in RPMI 1640 supplemented with 10% fetal bovine serum (FBS) and penicillin/streptomycin. HEK-293T and NIH-3T3 cells (American Type Culture Collection) were cultured in DMEM supplemented with 10% FBS and penicillin/streptomycin. Expansion of T-cell blasts were obtained by incubating PBMCs for 72 hours with PHA (2.5 µg/mL; Sigma-Aldrich) in Panserin 401 supplemented with 5% human male AB serum, and then with IL-2 (100 IU/mL, R&D Systems).

Plasmid constructs and lentiviral gene transfer

Human wild-type *IKZF1* cDNA was synthesized and subcloned into mammalian expression vector pcDNA3.1 (Invitrogen), pCMV3-HA or pFLAG-CMV2 (Origene). The plasmids containing different mutants of *IKZF1* were generated by mutagenesis using the Q5 Site-Directed Mutagenesis Kit (New England BioLabs) and verified by sequencing. cDNAs were inserted into a bicistronic lentiviral expression vector, pLVX-eF1a-IRES-mCherry (Clontech). HEK-293T cells were co-transfected with the lentiviral vector containing *IKZF1* with third-generation lentiviral plasmids containing Gag-Pol, Rev, and the G protein of the vesicular stomatitis virus. Supernatants containing virus particles were collected 72 h after transfection, and were concentrated by centrifugation. T cells were infected at day 1 of anti-CD3/CD28 beads stimulation with viral particles.

Immunoblotting

The plasmids containing WT or mutant *IKZF1* genes were transfected into HEK-293T cells with Lipofectamine 2000 (Thermo Fisher Scientific) according to the manufacturer's instructions. Cells were harvested 48 h post-transfection. The cytosolic proteins were extracted with cell membrane lysis buffer (10 mM HEPES, pH 7.9, 1.5 mM MgCl₂, 10 mM KCl, 0.1% NP40, protease inhibitor cocktail). Then, nuclei were pelleted and resuspended in nuclear lysis buffer (20 mM HEPES, pH 7.9, 25% glycerol, 420 mM NaCl, 1.5 mM MgCl₂, 0.2 mM EDTA, protease inhibitor cocktail) to obtain the nuclear protein extracts. Total cell lysates were obtained with TNE buffer (10 mM Tris, pH 7.8, 150 mM NaCl, 1 mM EDTA, 1% NP-40, protease inhibitor cocktail). Proteins were analyzed by standard SDS-PAGE and western blotting with the following antibodies: anti-*IKZF1* (ab191394, Abcam), anti-ACTIN (A2066, Sigma), anti-PCNA (2586, Cell Signaling Technology) and anti-KU80 antibody (2753, Cell Signaling Technology).

Electrophoresis mobility shift assay

2-6 µg nuclear protein extracts were incubated for 30 min at room temperature in HGDE buffer (20 mM HEPES, pH 7.9, 0.2 mM EDTA, 20% glycerol, 100 mM KCl, 1 mM DTT) with 1 µg poly(dI:dC), 1 µg bovine serum albumin, and 10 µM ZnCl₂, and then DY682 Infra-red dye-labeled double-strand probes were added. Samples were incubated for 25 min at room temperature. DNA-protein complexes were separated on 6% acrylamide gels with 0.5X TBE buffer. Gels were analyzed using an Odyssey CLx infrared scanner (Li-Cor). Anti- IKZF1 antibody (ab191394, Abcam) was used for the EMSA supershift assay. The sequence for probes were as follows: γ-Sat8 (forward: 5'-GCGAGACCGCAGGGAATGCTGGGAGCCTCCC-3'; reverse: 5'-GGGAGGCTCCCAGCATTCCCTGCGGTCTCGC-3'); IK-bs4 (forward: 5'-TGACAGGGAATACACATTCCCAAAGC-3'; reverse: 5'-GCTTTTGGGAATGTGTATTCCCTGTCA-3').

Immunoprecipitation

HEK-293T cells were co-transfected with pFLAG-CMV2-IKZF1 (WT) and pCMV3-HA-IKZF1 (WT or mutants) using Lipofectamine 2000. Cells were lysed in TNE buffer 24 h after transfection. Proteins were immunoprecipitated with Protein G-Sepharose 4 Fast Flow (GE Healthcare) and mouse anti-FLAG antibody (F3165, Sigma). Proteins were eluted by elution buffer (50 mM glycine, pH 2.8) and separated by standard SDS-PAGE. Then western blot analysis was performed using the rabbit anti-HA antibody (H6908, Sigma).

Confocal microscopic analysis

Immunofluorescence staining was performed using NIH-3T3 cells or T cells. The plasmids containing *IKZF1* cDNAs were transfected into NIH-3T3 cells on coverslips using Lipofectamine 2000, 48h prior to staining. T cells were stimulated with anti-CD3/CD28 activating Dynabeads (LifeTechnologies) for 24 h. Cells were fixed in 4% paraformaldehyde for 10 min, permeabilized with 0.1% Triton X-100 for 15 min, and incubated with anti-IKZF1 antibody (ab191394, Abcam). Alexa Flour 488-conjugated goat anti-rabbit IgG antibody (Invitrogen) were used as secondary antibodies. Cell nuclei were stained with 49-6-Diamidino-2-phenylindole. Images were acquired with a Leica SP8 STED confocal microscope (Leica Microsystems).

Luciferase reporter assay

HEK-293T cells were co-transfected with pcDNA3.1-IKZF1 (WT or mutants), pGL3 firefly luciferase reporter vector driven by the *HES1*(-872 to +299 bp), *MCL1*(-732 to +236 bp) or *MSH2* (-86 to +502 bp) promoters, and pRL-TK (Promega) using Lipofectamine 2000 24h before measurement of luciferase activity that was measured in triplicate using a Dual-Luciferase Reporter Assay System (Promega) and a multilabel reader (VICTO X4; PerkinElmer) according to the manufacturer's instructions.

Flow cytometry

For lymphocyte phenotyping, the following mAbs were used to stain the cell surface: anti-CD3 (SK7), anti-CD4 (RPA-T4), anti-CD8 (RPA-T8), anti-CD19 (SJ25C1), anti-CD20 (L27), anti-CD27 (LG.3A10), anti-CD38 (HIT2), anti-CD138 (MI15), anti-CD197/CCR7 (3D12), HLA-DR (G46-6) (BD Biosciences); anti-CD21 (BL13), anti-CD45RA (ALB11), anti-IgD (IA6-2) (Beckman Coulter); anti-CD11c (clone 3.9), anti-CD25 (BC96), anti-CD31 (WM59), anti-CD56 (HCD56) (Sony Biotechnology); anti-CD45RO (UCHL1) (Dako); anti-CD14 (HCD14), anti-CD16 (3G8), anti-CD57 (NK.1), anti-CD185/CCR5 (J252D4) (BioLegend); anti-CD20 (LT20),

anti-CD38 (IB6), anti-CD45 (5B1), anti-CD123 (AC145) (Miltenyi Biotec). For intracellular staining, cells were fixed and permeabilized with a FOXP3 staining kit (eBioscience) after surface staining, and stained with the following mAbs: anti-FOXP3 (259D/C7) (BD Pharmingen); anti-IRF4 (3E4) (eBioscience). Stained cells were analyzed with the BD LSRII-Fortessa (BD Biosciences), and data were processed with FlowJo software (Tree Star).

Proliferation assays

PBMCs were labeled with cell trace violet dye (1 μ M; Invitrogen) for 20 minutes at 37°C, and stimulated for 3 days with anti-CD3 mAb-coated plates (clone OKT3; eBioscience). IL-2 (100 IU/mL) or lenalidomide (10 μ M; Sigma) were added. Then cells were stained for CD4, CD8 and CD25 and analyzed by means of flow cytometry.

Cytokine expression

CD4⁺ naïve T cells (CD4⁺CD45RA⁺) were isolated from PBMCs by cell sorting using an SH800 cell sorter (SONY). Cells were transfected with lentiviral particles carrying IKZF1 (WT or mutant)-IRES-mCherry plasmid, and mCherry⁺ cells were sorted by 3 days after infection. The purity of CD4⁺CD45RA⁺ T cells and mCherry⁺ T cells were >98% and >96%, respectively, as assessed by flow cytometry. Cells were cultured with anti-CD3 mAb-coated plates for total 7 days. Those cells or day-7 T-cell blasts were used for cytokine expression. T cells were re-stimulated with PMA (100 ng/mL; Sigma-Aldrich) and ionomycin (1 μ g/mL; Sigma-Aldrich) for 6 h or overnight at 37°C in the presence of brefeldin A. Cells were fixed and permeabilized with the BD Cytotfix/Cytoperm Plus kit (BD Pharmingen) after surface staining, and stained with the following mAbs: anti-IL-2 (MQ1-17H12), anti-IFN- γ (4S.B3) (BioLegend); anti-IL-4 (8D4-8) (eBioscience).

Gene expression analysis

Total RNA was extracted using a Pure Link RNA Mini kit (Thermo Fisher Scientific) and cDNA was generated by a first-strand synthesis system (SuperScript II; Thermo Fisher Scientific). Real-time quantitative PCR was performed using a real-time PCR system (ViiA 7; Thermo Fisher Scientific) and an assay-on-demand Taqman probe and primers (Hs00894392 for *TBX21*, Hs00231122 for *GATA3*, Hs00193519 for *MAF* and Hs99999905 for *GAPDH*; Applied Biosystems), according to the manufacturer's instructions. Relative expression levels were normalized to *GAPDH* and analyzed by the $\Delta\Delta C_t$ method.

Treg and PC differentiation assays

CD4⁺ Naïve T cells (CD4⁺CD45RA⁺CCR7⁺CD25⁻) or memory B cells (CD19⁺CD27⁺) were isolated by cell sorting from PBMCs. The purities of CD4⁺CD45RA⁺CCR7⁺CD25⁻ T cells or CD19⁺CD27⁺ B cells were >97% and >98% respectively. CD4⁺CD45RA⁺CCR7⁺CD25⁻ cells were cultured with anti-CD3 mAb-coated plates (10 μ g/mL), anti-CD28 mAb (1 μ g/mL; BD Pharmingen) and TGF- β 1 (5 ng/mL; peprotech) in the presence or absence of IL-2 (100 IU/mL). At day 6, cells were stained for FOXP3 and analyzed by means of flow cytometry. As previously described (27), CD19⁺CD27⁺ cells were cultured with CpG (10 μ g/mL; Sigma-Aldrich), CD40 ligand (50 ng/mL; R&D Systems), IL-2 (20 IU/mL), IL-10 (50 ng/mL; R&D Systems) and IL-15 (10 ng/mL; R&D Systems) for 4 days, IL-2 (20 IU/mL), IL-6 (50 ng/mL; R&D Systems), IL-10 (50 ng/mL) and IL-15 (10 ng/mL) for 3 days, and IL-6 (50 ng/mL), IL-15 (10 ng/mL) and IFN- α (500 IU/mL; R&D Systems) for 3 days in the presence or absence of lenalidomide (10 μ M). At

day 10, cells were stained for CD20, CD38, CD138 and IRF4 and analyzed by means of flow cytometry.

Immunohistochemistry

Pathological analysis was performed on cervical lymph node tissue using conventional hematoxylin and eosin staining. For immunohistochemical analysis, antibodies against IgG4 (1:200; clone MRQ-44; Cell Marque, Rocklin, CA, USA) and MUM1 (1:100; clone MUM1p; Agilent Dako, Santa Clara, CA, USA) were used.

Statistics

All values were presented as mean \pm SD. Comparison between groups were analyzed with one-way ANOVA with Dunnett's post hoc multiple-comparisons test or Holm-Šidák multiple-comparisons test, Mann-Whitney U test, or chi-square test using GraphPad Prism 8 software (GraphPad). When P was less than 0.05, the differences were considered significant.

Supplementary Materials

Fig. S1. In silico analysis

Fig. S2. Subcellular localization and dimerization

Fig. S3. Immune phenotyping of PBMCs

Fig. S4. Proliferation, differentiation and cytokine productions of T cells

Fig. S5 Schematic diagram of IKZF1 roles in T/B-cell development.

Table S1. Total and specific immunoglobulin levels and post vaccination serologies

Table S2. Immunological features of peripheral blood from patients with *IKZF1*^{R183H/C} variants

Table S3. *IKZF1* somatic variants in BCP-ALL or MM

References and Notes

1. K. Georgopoulos, M. Bigby, J.-H. Wang, A. Molnar, P. Wu, S. Winandy, A. H. Sharpe, The Ikaros gene is required for the development of all lymphoid lineages. *Cell*. **79**, 143–156 (1994).
2. B. Heizmann, P. Kastner, S. Chan, The Ikaros family in lymphocyte development. *Curr Opin Immunol*. **51**, 14–23 (2018).
3. T. A. Schwickert, H. Tagoh, S. Gültekin, A. Dakic, E. Axelsson, M. Minnich, A. Ebert, B. Werner, M. Roth, L. Cimmino, R. A. Dickins, J. Zuber, M. Jaritz, M. Busslinger, Stage-specific control of early B cell development by the transcription factor Ikaros. *Nat Immunol*. **15**, 283–293 (2014).
4. J.-H. Wang, A. Nichogiannopoulou, L. Wu, L. Sun, A. H. Sharpe, M. Bigby, K. Georgopoulos, Selective Defects in the Development of the Fetal and Adult Lymphoid System in Mice with an Ikaros Null Mutation. *Immunity*. **5**, 537–549 (1996).

5. P. Papathanasiou, A. C. Perkins, B. S. Cobb, R. Ferrini, R. Sridharan, G. F. Hoyne, K. A. Nelms, S. T. Smale, C. C. Goodnow, Widespread Failure of Hematolymphoid Differentiation Caused by a Recessive Niche-Filling Allele of the Ikaros Transcription Factor. *Immunity*. **19**, 131–144 (2003).
6. M. L. Churchman, M. Qian, G. te Kronnie, R. Zhang, W. Yang, H. Zhang, T. Lana, P. Tedrick, R. Baskin, K. Verbist, J. L. Peters, M. Devidas, E. Larsen, I. M. Moore, Z. Gu, C. Qu, H. Yoshihara, S. N. Porter, S. M. Pruett-Miller, G. Wu, E. Raetz, P. L. Martin, W. P. Bowman, N. Winick, E. Mardis, R. Fulton, M. Stanulla, W. E. Evans, M. V. Relling, C.-H. Pui, S. P. Hunger, M. L. Loh, R. Handgretinger, K. E. Nichols, J. J. Yang, C. G. Mullighan, Germline Genetic IKZF1 Variation and Predisposition to Childhood Acute Lymphoblastic Leukemia. *Cancer Cell*. **33**, 937-948.e8 (2018).
7. L. Olsson, B. Johansson, Ikaros and leukaemia. *Br J Haematol*. **169**, 479–491 (2015).
8. H. S. Kuehn, B. Boisson, C. Cunningham-Rundles, J. Reichenbach, A. Stray-Pedersen, E. W. Gelfand, P. Maffucci, K. R. Pierce, J. K. Abbott, K. V. Voelkerding, S. T. South, N. H. Augustine, J. S. Bush, W. K. Dolen, B. B. Wray, Y. Itan, A. Cobat, H. S. Sorte, S. Ganesan, S. Prader, T. B. Martins, M. G. Lawrence, J. S. Orange, K. R. Calvo, J. E. Niemela, J.-L. Casanova, T. A. Fleisher, H. R. Hill, A. Kumánovics, M. E. Conley, S. D. Rosenzweig, Loss of B Cells in Patients with Heterozygous Mutations in IKAROS. *N Engl J Med*. **374**, 1032–1043 (2016).
9. A. Hoshino, S. Okada, K. Yoshida, N. Nishida, Y. Okuno, H. Ueno, M. Yamashita, T. Okano, M. Tsumura, S. Nishimura, S. Sakata, M. Kobayashi, H. Nakamura, J. Kamizono, K. Mitsui-Sekinaka, T. Ichimura, S. Ohga, Y. Nakazawa, M. Takagi, K. Imai, Y. Shiraishi, K. Chiba, H. Tanaka, S. Miyano, S. Ogawa, S. Kojima, S. Nonoyama, T. Morio, H. Kanegane, Abnormal hematopoiesis and autoimmunity in human subjects with germline IKZF1 mutations. *J Allergy Clin Immunol*. **140**, 223–231 (2017).
10. D. Boutboul, H. S. Kuehn, Z. Van de Wyngaert, J. E. Niemela, I. Callebaut, J. Stoddard, C. Lenoir, V. Barlogis, C. Farnarier, F. Vely, N. Yoshida, S. Kojima, H. Kanegane, A. Hoshino, F. Hauck, L. Lhermitte, V. Asnafi, P. Roehrs, S. Chen, J. W. Verbsky, K. R. Calvo, A. Husami, K. Zhang, J. Roberts, D. Amrol, J. Sleaseman, A. P. Hsu, S. M. Holland, R. Marsh, A. Fischer, T. A. Fleisher, C. Picard, S. Latour, S. D. Rosenzweig, Dominant-negative IKZF1 mutations cause a T, B, and myeloid cell combined immunodeficiency. *J Clin Invest*. **128**, 3071–3087 (2018).
11. H. S. Kuehn, J. E. Niemela, J. Stoddard, S. C. Mannurita, T. Shahin, S. Goel, M. Hintermeyer, R. J. Heredia, M. Garofalo, L. Lucas, S. Singh, A. Tondo, Z. Jacobs, W. A. Gahl, S. Latour, J. Verbsky, J. Routes, C. Cunningham-Rundles, K. Boztug, E. Gambineri, T. A. Fleisher, S. Chandrakasan, S. D. Rosenzweig, Germline IKAROS dimerization haploinsufficiency causes hematologic cytopenias and malignancies. *Blood*. **137**, 349–363 (2021).
12. J. Hadjadj, N. Aladjidi, H. Fernandes, G. Leverger, A. Magérus-Chatinet, F. Mazerolles, M.-C. Stolzenberg, S. Jacques, C. Picard, J. Rosain, C. Fournage, S. Hanein, M. Zarhrate, M. Pasquet, W. Abou Chahla, V. Barlogis, Y. Bertrand, I. Pellier, E. Colomb Bottollier, F.

- Fouyssac, P. Blouin, C. Thomas, N. Cheikh, E. Dore, C. Pondarre, D. Plantaz, E. Jeziorski, F. Millot, N. Garcelon, S. Ducassou, Y. Perel, T. Leblanc, B. Neven, A. Fischer, F. Rieux-Laucat, Pediatric Evans syndrome is associated with a high frequency of potentially damaging variants in immune genes. *Blood*. **134**, 9–21 (2019).
13. A. Patel, H. Hashimoto, X. Zhang, X. Cheng, in *Methods in Enzymology* (Elsevier, 2016; <https://linkinghub.elsevier.com/retrieve/pii/S0076687916000641>), vol. 573, pp. 387–401.
 14. A. Patel, P. Yang, M. Tinkham, M. Pradhan, M.-A. Sun, Y. Wang, D. Hoang, G. Wolf, J. R. Horton, X. Zhang, T. Macfarlan, X. Cheng, DNA Conformation Induces Adaptable Binding by Tandem Zinc Finger Proteins. *Cell*. **173**, 221-233.e12 (2018).
 15. A. Patel, X. Zhang, R. M. Blumenthal, X. Cheng, Structural basis of human PR/SET domain 9 (PRDM9) allele C-specific recognition of its cognate DNA sequence. *J Biol Chem*. **292**, 15994–16002 (2017).
 16. I. Iacobucci, N. Iraci, M. Messina, A. Lonetti, S. Chiaretti, E. Valli, A. Ferrari, C. Papayannidis, F. Paoloni, A. Vitale, C. T. Storlazzi, E. Ottaviani, V. Guadagnuolo, S. Durante, M. Vignetti, S. Soverini, F. Pane, R. Foà, M. Baccarani, M. Müschen, G. Perini, G. Martinelli, IKAROS Deletions Dictate a Unique Gene Expression Signature in Patients with Adult B-Cell Acute Lymphoblastic Leukemia. *PLoS ONE*. **7**, e40934 (2012).
 17. A. Apostolov, I. Litim-Mecheri, A. Oravec, M. Goepf, P. Kirstetter, P. Marchal, A. Ittel, L. Mauvieux, S. Chan, P. Kastner, Sumoylation Inhibits the Growth Suppressive Properties of Ikaros. *PLoS ONE*. **11**, e0157767 (2016).
 18. S. O'Brien, R. M. Thomas, G. B. Wertheim, F. Zhang, H. Shen, A. D. Wells, Ikaros Imposes a Barrier to CD8⁺ T Cell Differentiation by Restricting Autocrine IL-2 Production. *J Immunol*. **192**, 5118–5129 (2014).
 19. Z. Eskandarian, M. Fliegau, A. Bulashevskaya, M. Proietti, R. Hague, C. R. Smulski, D. Schubert, K. Warnatz, B. Grimbacher, Assessing the Functional Relevance of Variants in the IKAROS Family Zinc Finger Protein 1 (IKZF1) in a Cohort of Patients With Primary Immunodeficiency. *Front Immunol*. **10**, 568 (2019).
 20. J. Geginat, A. Lanzavecchia, F. Sallusto, Proliferation and differentiation potential of human CD8⁺ memory T-cell subsets in response to antigen or homeostatic cytokines. *Blood*. **101**, 4260–4266 (2003).
 21. M. R. Quirion, G. D. Gregory, S. E. Umetsu, S. Winandy, M. A. Brown, Cutting Edge: Ikaros Is a Regulator of Th2 Cell Differentiation. *J Immunol*. **182**, 741–745 (2009).
 22. R. M. Thomas, C. Chen, N. Chunder, L. Ma, J. Taylor, E. J. Pearce, A. D. Wells, Ikaros Silences T-bet Expression and Interferon- γ Production during T Helper 2 Differentiation. *J Biol Chem*. **285**, 2545–2553 (2010).
 23. R. M. Thomas, N. Chunder, C. Chen, S. E. Umetsu, S. Winandy, A. D. Wells, Ikaros Enforces the Costimulatory Requirement for *IL2* Gene Expression and Is Required for Anergy

- Induction in CD4⁺ T Lymphocytes. *J Immunol.* **179**, 7305–7315 (2007).
24. J. D. Fontenot, J. P. Rasmussen, M. A. Gavin, A. Y. Rudensky, A function for interleukin 2 in Foxp3-expressing regulatory T cells. *Nat Immunol.* **6**, 1141–1152 (2005).
 25. A. Ballesteros-Tato, B. León, B. A. Graf, A. Moquin, P. S. Adams, F. E. Lund, T. D. Randall, Interleukin-2 Inhibits Germinal Center Formation by Limiting T Follicular Helper Cell Differentiation. *Immunity.* **36**, 847–856 (2012).
 26. M. Miyara, Y. Yoshioka, A. Kitoh, T. Shima, K. Wing, A. Niwa, C. Parizot, C. Taflin, T. Heike, D. Valeyre, A. Mathian, T. Nakahata, T. Yamaguchi, T. Nomura, M. Ono, Z. Amoura, G. Gorochoy, S. Sakaguchi, Functional Delineation and Differentiation Dynamics of Human CD4⁺ T Cells Expressing the FoxP3 Transcription Factor. *Immunity.* **30**, 899–911 (2009).
 27. M. Jourdan, M. Cren, P. Schafer, N. Robert, C. Duperray, L. Vincent, P. Ceballos, G. Cartron, J.-F. Rossi, J. Moreaux, R. Chopra, B. Klein, Differential effects of lenalidomide during plasma cell differentiation. *Oncotarget.* **7**, 28096–28111 (2016).
 28. J. Kronke, N. D. Udeshi, A. Narla, P. Grauman, S. N. Hurst, M. McConkey, T. Svinkina, D. Heckl, E. Comer, X. Li, C. Ciarlo, E. Hartman, N. Munshi, M. Schenone, S. L. Schreiber, S. A. Carr, B. L. Ebert, Lenalidomide Causes Selective Degradation of IKZF1 and IKZF3 in Multiple Myeloma Cells. *Science.* **343**, 301–305 (2014).
 29. G. Lu, R. E. Middleton, H. Sun, M. Naniong, C. J. Ott, C. S. Mitsiades, K.-K. Wong, J. E. Bradner, W. G. Kaelin, The Myeloma Drug Lenalidomide Promotes the Cereblon-Dependent Destruction of Ikaros Proteins. *Science.* **343**, 305–309 (2014).
 30. K. G. Roberts, Y. Li, D. Payne-Turner, R. C. Harvey, Y.-L. Yang, D. Pei, K. McCastlain, L. Ding, C. Lu, G. Song, J. Ma, J. Becksfort, M. Rusch, S.-C. Chen, J. Easton, J. Cheng, K. Boggs, N. Santiago-Morales, I. Iacobucci, R. S. Fulton, J. Wen, M. Valentine, C. Cheng, S. W. Paugh, M. Devidas, I.-M. Chen, S. Reshmi, A. Smith, E. Hedlund, P. Gupta, P. Nagahawatte, G. Wu, X. Chen, D. Yergeau, B. Vadodaria, H. Mulder, N. J. Winick, E. C. Larsen, W. L. Carroll, N. A. Heerema, A. J. Carroll, G. Grayson, S. K. Tasian, A. S. Moore, F. Keller, M. Frei-Jones, J. A. Whitlock, E. A. Raetz, D. L. White, T. P. Hughes, J. M. Guidry Auvil, M. A. Smith, G. Marcucci, C. D. Bloomfield, K. Mrózek, J. Kohlschmidt, W. Stock, S. M. Kornblau, M. Konopleva, E. Paietta, C.-H. Pui, S. Jeha, M. V. Relling, W. E. Evans, D. S. Gerhard, J. M. Gastier-Foster, E. Mardis, R. K. Wilson, M. L. Loh, J. R. Downing, S. P. Hunger, C. L. Willman, J. Zhang, C. G. Mullighan, Targetable Kinase-Activating Lesions in Ph-like Acute Lymphoblastic Leukemia. *N Engl J Med.* **371**, 1005–1015 (2014).
 31. T. Lana, P. de Lorenzo, S. Bresolin, I. Bronzini, M. L. den Boer, H. Cavé, E. Froňková, M. Stanulla, M. Zaliova, C. J. Harrison, H. de Groot, M. G. Valsecchi, A. Biondi, G. Basso, G. Cazzaniga, G. te Kronnie, Refinement of IKZF1 status in pediatric Philadelphia-positive acute lymphoblastic leukemia. *Leukemia.* **29**, 2107–2110 (2015).
 32. J. F. Li, Y. T. Dai, H. Lilljebjörn, S. H. Shen, B.-W. Cui, L. Bai, Y. F. Liu, M. X. Qian, Y. Kubota, H. Kiyoi, I. Matsumura, Y. Miyazaki, L. Olsson, A. M. Tan, H. Ariffin, J. Chen, J. Takita, T. Yasuda, H. Mano, B. Johansson, J. J. Yang, A. E. J. Yeoh, F. Hayakawa, Z. Chen,

- C. H. Pui, T. Fioretos, S. J. Chen, J. Y. Huang, Transcriptional landscape of B cell precursor acute lymphoblastic leukemia based on an international study of 1,223 cases. *Proc Natl Acad Sci USA*. **115**, E11711–E11720 (2018).
33. S. Barrio, U. Munawar, Y. X. Zhu, N. Giesen, C.-X. Shi, M. D. Viá, R. Sanchez, L. Bruins, T. Demler, N. Müller, L. Haertle, A. Garitano, T. Steinbrunn, S. Danhof, I. Cuenca, C. Barrio-Garcia, E. Braggio, A. Rosenwald, J. Martinez-Lopez, L. Rasche, M. S. Raab, A. K. Stewart, H. Einsele, T. Stühmer, K. M. Kortüm, IKZF1/3 and CRL4^{CRBN} E3 ubiquitin ligase mutations and resistance to immunomodulatory drugs in multiple myeloma. *Haematologica*. **105**, e237–e241 (2020).
 34. C. C. Bjorklund, L. Lu, J. Kang, P. R. Hagner, C. G. Havens, M. Amatangelo, M. Wang, Y. Ren, S. Couto, M. Breider, Y. Ning, A. K. Gandhi, T. O. Daniel, R. Chopra, A. Klippel, A. G. Thakurta, Rate of CRL4CRBN substrate Ikaros and Aiolos degradation underlies differential activity of lenalidomide and pomalidomide in multiple myeloma cells by regulation of c-Myc and IRF4. *Blood Cancer J*. **5**, e354–e354 (2015).
 35. C. Lyon de Ana, K. Arakcheeva, P. Agnihotri, N. Derosia, S. Winandy, Lack of Ikaros Deregulates Inflammatory Gene Programs in T Cells. *J Immunol*. **202**, 1112–1123 (2019).
 36. S. E. Umetsu, S. Winandy, Ikaros Is a Regulator of *Il10* Expression in CD4⁺ T Cells. *J Immunol*. **183**, 5518–5525 (2009).
 37. R. Bianchini, S. N. Karagiannis, G. Jordakieva, E. Jensen-Jarolim, The Role of IgG4 in the Fine Tuning of Tolerance in IgE-Mediated Allergy and Cancer. *Int J Mol Sci*. **21**, 5017 (2020).
 38. D. J. Bogaert, H. S. Kuehn, C. Bonroy, K. R. Calvo, J. Dehoorne, A. V. Vanlander, M. De Bruyne, U. Cytlak, V. Bigley, F. De Baets, E. De Baere, S. D. Rosenzweig, F. Haerynck, M. Dullaers, A novel IKAROS haploinsufficiency kindred with unexpectedly late and variable B-cell maturation defects. *J Allergy Clin Immunol*. **141**, 432-435.e7 (2018).
 39. E. Van Nieuwenhove, J. E. Garcia-Perez, C. Helsen, P. D. Rodriguez, P. A. van Schouwenburg, J. Dooley, S. Schlenner, M. van der Burg, E. Verhoeyen, R. Gijssbers, S. Fietze, H. Schjerven, I. Meyts, F. Claessens, S. Humblet-Baron, C. Wouters, A. Liston, A kindred with mutant IKAROS and autoimmunity. *J Allergy Clin Immunol*. **142**, 699-702.e12 (2018).
 40. D. J. Groth, M. M. Lakkaraja, J. O. Ferreira, E. J. Feuille, J. A. Bassetti, S. M. Kaicker, Management of chronic immune thrombocytopenia and presumed autoimmune hepatitis in a child with IKAROS haploinsufficiency. *J Clin Immunol*. **40**, 653–657 (2020).
 41. T. A. Schwickert, H. Tagoh, K. Schindler, M. Fischer, M. Jaritz, M. Busslinger, Ikaros prevents autoimmunity by controlling anergy and Toll-like receptor signaling in B cells. *Nat Immunol*. **20**, 1517–1529 (2019).
 42. S. G. Tangye, W. Al-Herz, A. Bousfiha, T. Chatila, C. Cunningham-Rundles, A. Etzioni, J. L. Franco, S. M. Holland, C. Klein, T. Morio, H. D. Ochs, E. Oksenhendler, C. Picard, J. Puck, T. R. Torgerson, J.-L. Casanova, K. E. Sullivan, Human Inborn Errors of Immunity: 2019

Update on the Classification from the International Union of Immunological Societies Expert Committee. *J Clin Immunol.* **40**, 24–64 (2020).

Acknowledgements: We acknowledge the patients, their families, and healthy donors for their cooperation and blood donation. We thank Annarita Miccio, Vasco Meneghini and Giacomo Frati (Institut Imagine, Paris) for their help and discussion. S. Latour is a senior scientist at the Centre National de la Recherche Scientifique (France). A.H. and D.B. were supported by the Agence Nationale de Recherche (ANR, France). J.H. was a recipient of an Institut National de la Santé et de la Recherche Médicale/INSERM “poste d’accueil” program, and from the Institute Imagine MD-PhD fellowship program supported by the Fondation Bettencourt Schueller.

Fundings:

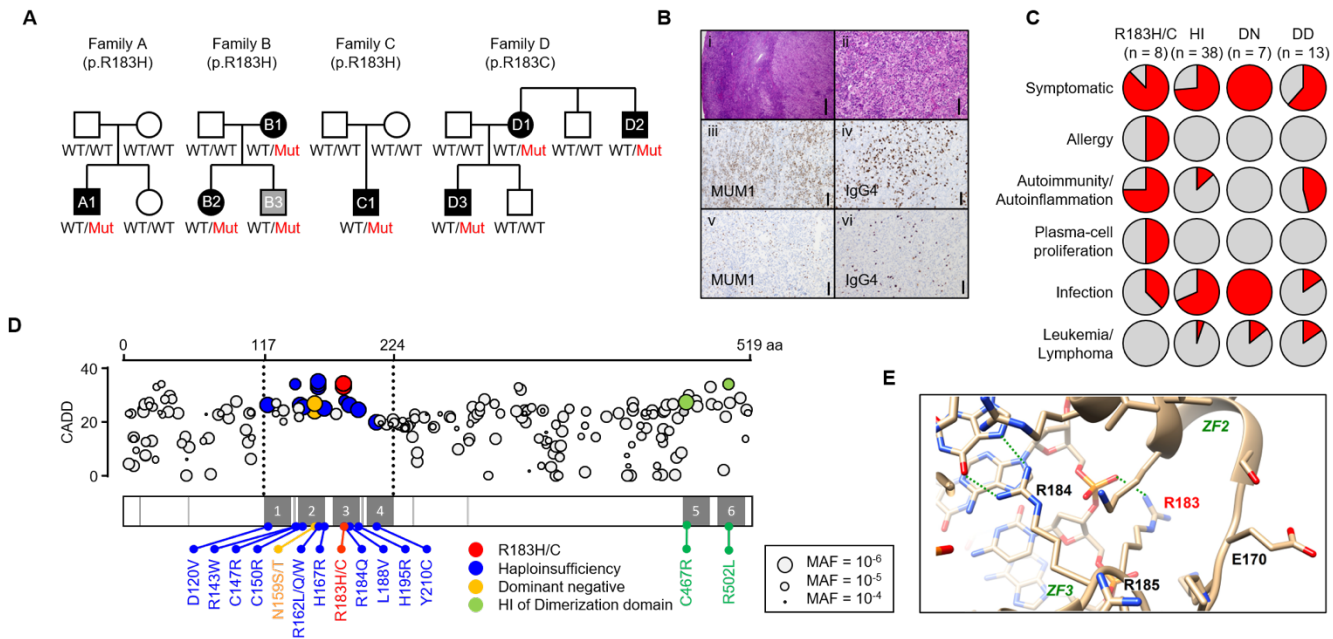
Ligue Contre le Cancer-Equipe Labelisée (SL)
The Rare Diseases Foundation (SL)
INSERM (SL)
ANR grant ANR-18-CE15-0025-01 (SL)
ANR grant ANR-14-CE14-0026-01(FRL)
ANR grant ANR-18-CE17-0001 (FRL)
ANR grant ANR-18-RHUS-0010 (FRL)
ANR grant ANR-10-IAHU-01 (Institut Imagine)
Société Française de Lutte contre les Cancers et Leucémies de l’Enfant/AREMIG (SL)
German Centre for Infection Research DZIF grant TTU 07.909 (FH)
Else Kröner-Fresenius Stiftung grant EKFS, 2017_A110 (FH)
German Federal Ministry of Education and Research grant BMBF, 01GM1910C (FH)

Author contributions: AH and DB designed, performed experiments and analyzed the data. YZ, HSK, CW, IC, CL performed experiments and analyzed the data. JH, IÖ, TC, NM, CK, XP, AA, ER, MC, FR-L, FH, JM and SDR identified the patients and provided clinical and exome data. CP, AF, FH, JM and SDR analyzed the data. AH and SL wrote the manuscript. SL designed and supervised the research.

Competing interests: The authors have no conflicts of interest to declare.

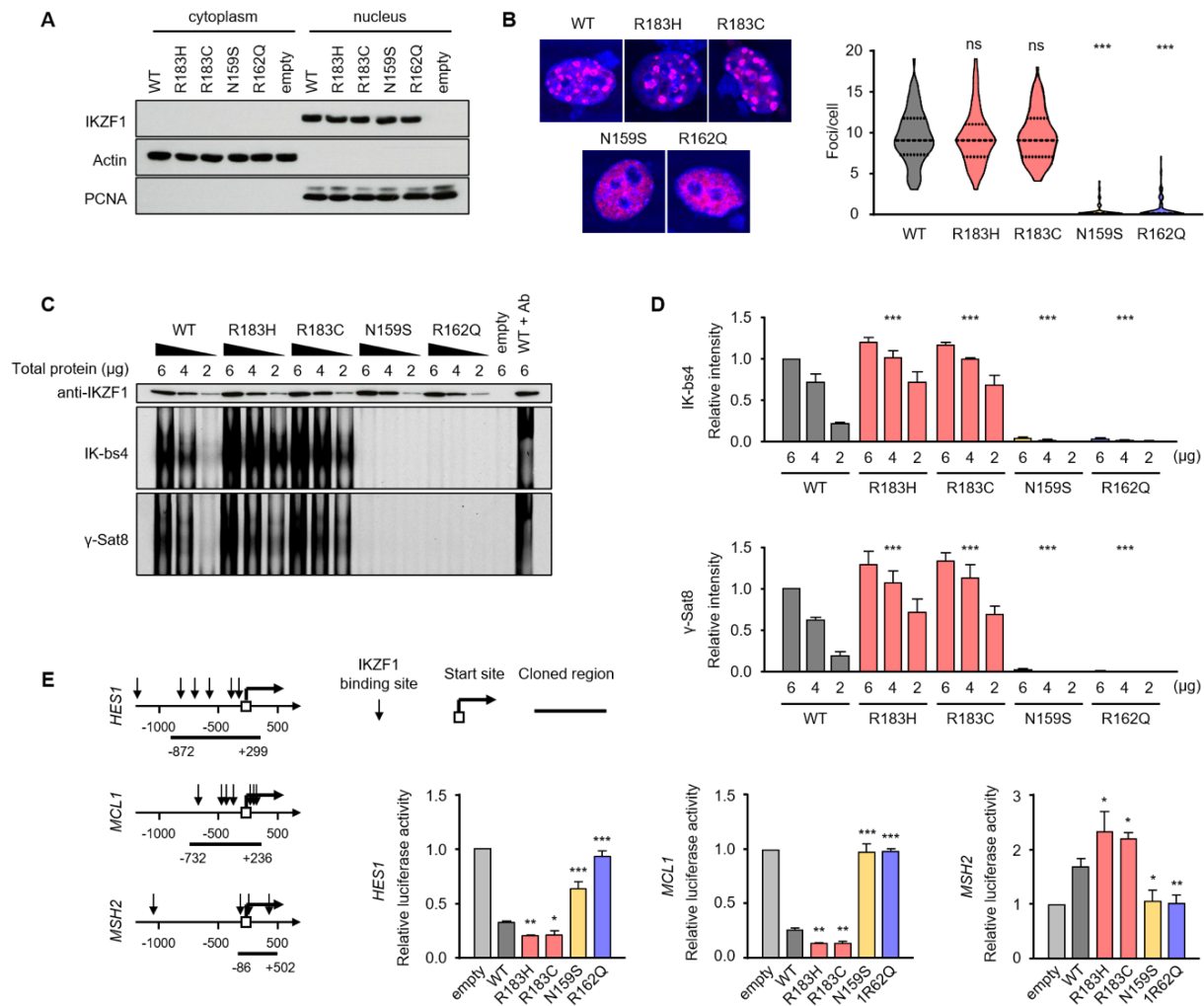
Data and materials availability: All data and materials used in the analysis are available and requests can be sent to Sylvain Latour.

Fig.1 Identification of heterozygous *IKZF1*^{R183H} and *IKZF1*^{R183C} variants



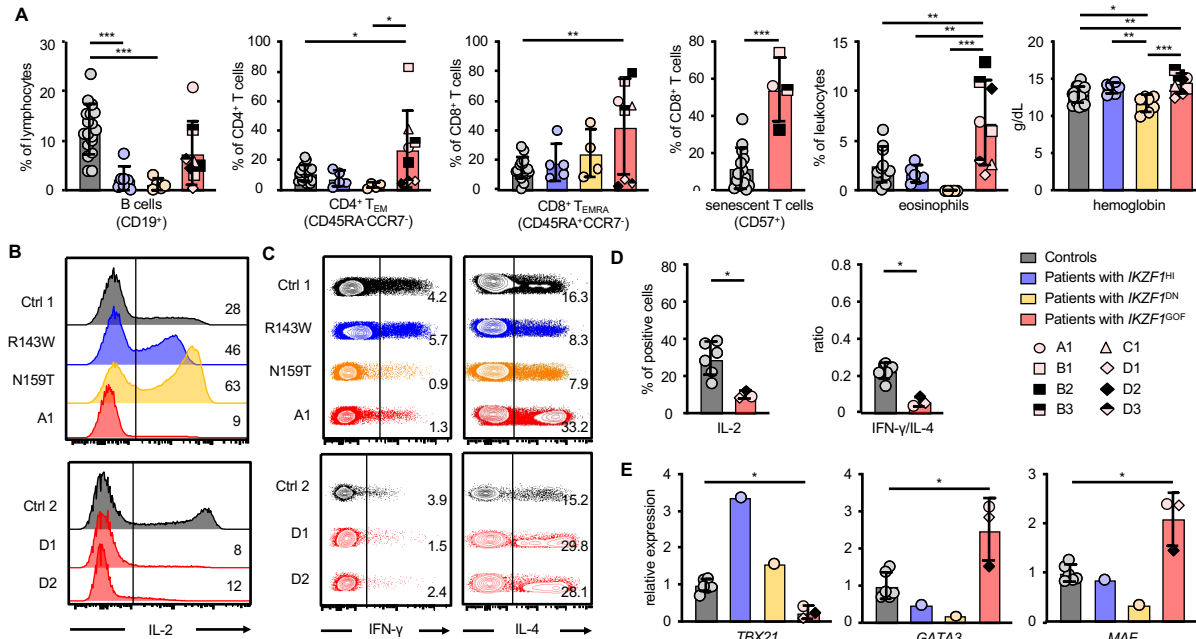
(A) Pedigrees of 4 families with heterozygous *IKZF1*^{R183H} or *IKZF1*^{R183C} variants. Non-affected, affected and asymptomatic individuals in white, black and gray respectively. WT, wild-type allele ; Mut (in red), mutated allele. **(B)** Immunohistochemistry of lymph nodes from B1 (i-iv) and B2 (v,vi) showing lymphoid tissues without visible follicles and massive dilatation of sinuses (i) that are densely packed with monohistiocytic cells and lymphocytic cells (ii) with accumulation of plasma cells stained with MUM1/IRF4 (iii,v) and IgG4 (iv,vi). Scale bars for 500µm in (i) and 100µm in (ii-vi). **(C)** Clinical manifestations in patients with *IKZF1*^{R183H/C}, *IKZF1*^{HI}, *IKZF1*^{DN} or *IKZF1*^{DD}. Positive manifestations are shown in red. **(D)** IKZF1 protein structure and predicted combined annotation dependent depletion (CADD) scores with R183H and R183C variants (red), known missense *IKZF1*^{HI} (blue), *IKZF1*^{DN} (yellow) and *IKZF1*^{DD} (green) variants, and missense variants reported in the gnomAD (gray). Circles correspond to minor allele frequencies (MAF). **(E)** Model of the 3D structure of human IKZF1 ZF3, using as a template the 3D structure of Zfp568 ZF7 complexed with DNA (pdb 5V3J). Additional bonds may occur with main carbonyl atoms of the chain linking ZF2 to ZF3, depending on the position of the R183 side chain.

Fig. 2. IKZF1^{R183H/C} variants behave as gain-of-function



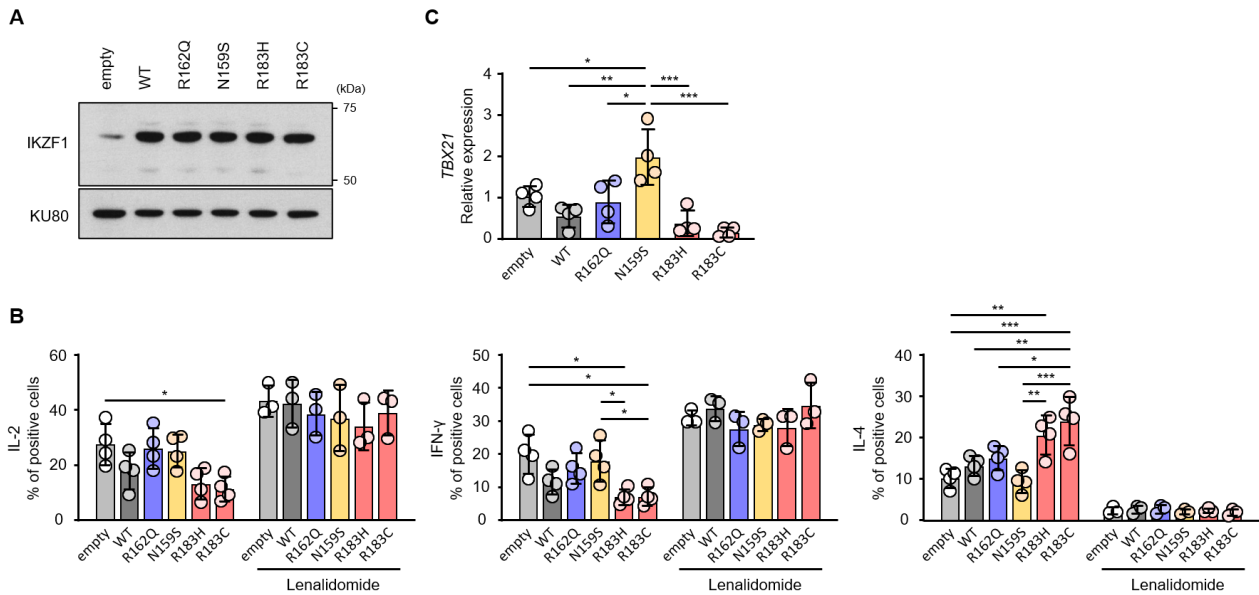
(A) Immunoblots of IKZF1 nuclear and cytoplasm expression in HEK-293T cells transiently expressing IKZF1^{WT}, IKZF1^{R183H}, IKZF1^{R183C}, IKZF1^{N159S} (IKZF1^{DN}), IKZF1^{R162Q} (IKZF1^{HI}), or empty vector. Anti-Actin and anti-PCNA as cytoplasm and nucleus loading control respectively. **(B)** IKZF1 localization in NIH-3T3 cells transiently expressing IKZF1^{WT} or same mutants as in (A). Staining with anti-IKZF1 (red) and DAPI (blue) (left panel). IKZF1 foci counts from 100 cells for each condition (right panel). **(C)** EMSA with nuclear extracts from HEK-293T cells as in (A). Immunoblot of IKZF1 expression (upper panel) and EMSA with IK-bs4 (middle panel) or γ -Sat8 (lower panel) probes. Anti-IKZF1 induced a supershift as control (WT+Ab). **(D)** Graphs of EMSA quantifications. Relative intensities with IKZF1^{WT} (6 μ g) defined as 1. **(E)** Relative luciferase activities of *HES1*, *MCL1* or *MSH2* promoter constructs when co-transfected in HEK-293T with IKZF1^{WT} and same mutants as in (A) and compared to those with the empty vector. Diagrams of cloned promoters with IKZF1 binding sites (left panel). In (D) and (E), data presented as mean \pm SD of 3 independent experiments. Comparison between groups in (B), (D) and (E) analyzed with one-way ANOVA with Dunnett's post hoc multiple-comparisons test. *P < 0.05, **P < 0.01, ***P < 0.001.

Fig. 3. *IKZF1*^{GOF} variants result in aberrant cytokine productions and Th differentiation



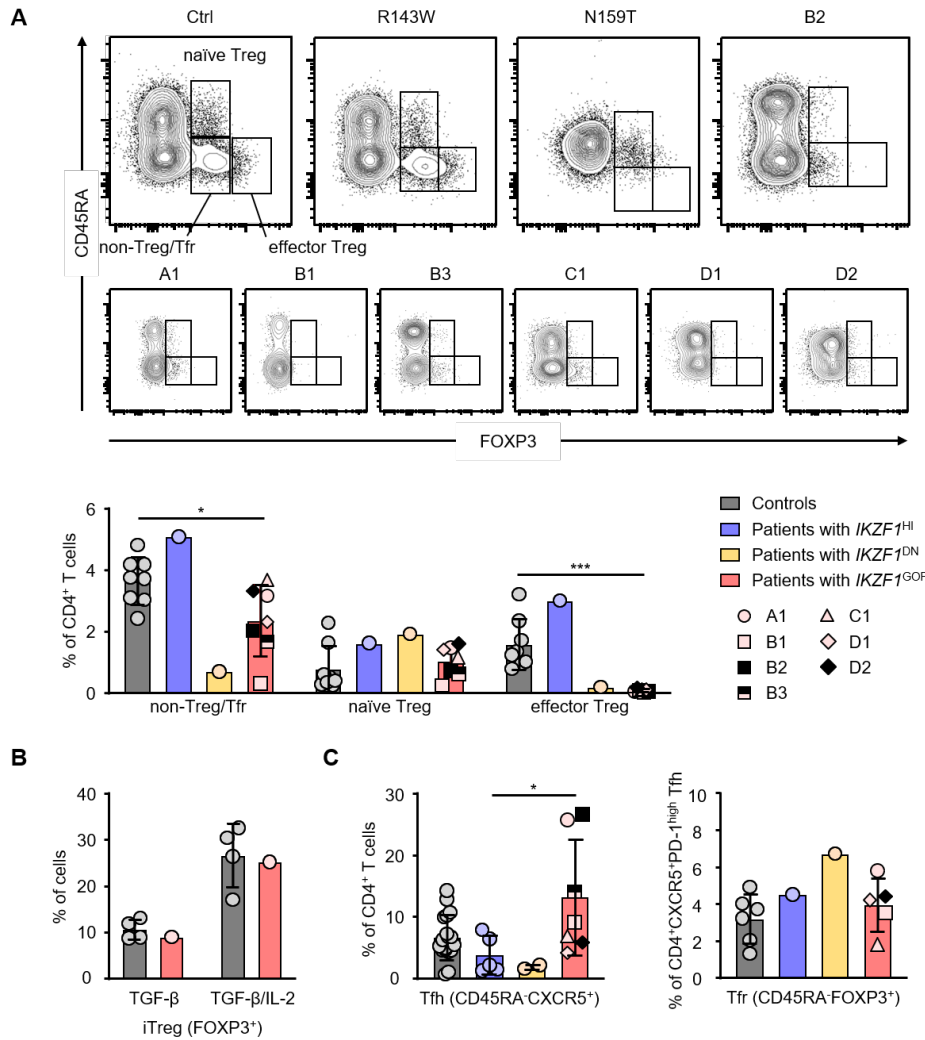
(A) Graph bars showing frequencies of B cells ; effector memory T cells/ T_{EM} ; terminally differentiated effector memory T cells/ T_{EMRA} ,; senescence T cells ; eosinophils and hemoglobin levels in controls, *IKZF1*^{HI} (C147R, R162Q and R162W), *IKZF1*^{DN} (N159S/T) and *IKZF1*^{GOF} (R183H/C) patients. (B) Histograms of IL-2 intracellular production by T-cell blasts stimulated with PMA+ionomycin for 6 h gated on CD4⁺ T cells of controls, *IKZF1*^{HI} (R143W), *IKZF1*^{DN} (N159T) and *IKZF1*^{GOF} (A1, D1 and D2) patients. (C) Same as in (B) excepted that cells were analyzed for IFN- γ (left panel) or IL-4 (right panel) intracellular production after overnight stimulation. (D) Graphs of frequencies of IL-2-positive cells and ratios of IFN- γ /IL-4-positive cells from (B, C). (E) Same as in (C) excepted that the mRNA expression of *TBX21*, *GATA3* and *MAF* was analyzed by qPCR. Data normalized on *GAPDH* mRNA expression. (A-D) Data from FACS analyses. (B, C) Two independent experiments shown and numbers indicate the percentage of IL-2, IFN- γ - or IL-4-positive cells. In (A), (D) and (E), data presented as mean \pm SD. Comparison between groups analyzed with one-way ANOVA with Holm-Šidák multiple-comparisons test in (A) and Mann-Whitney *U* test in (D) and (E). **P* < 0.05, ***P* < 0.01, ****P* < 0.001.

Fig. 4. Expression of IKZF1^{GOF} inhibits IL-2 and induces Th2 skewing in T cells
(A-C) CD4⁺ naïve T cells from healthy controls were infected with lentiviral vector-encoding



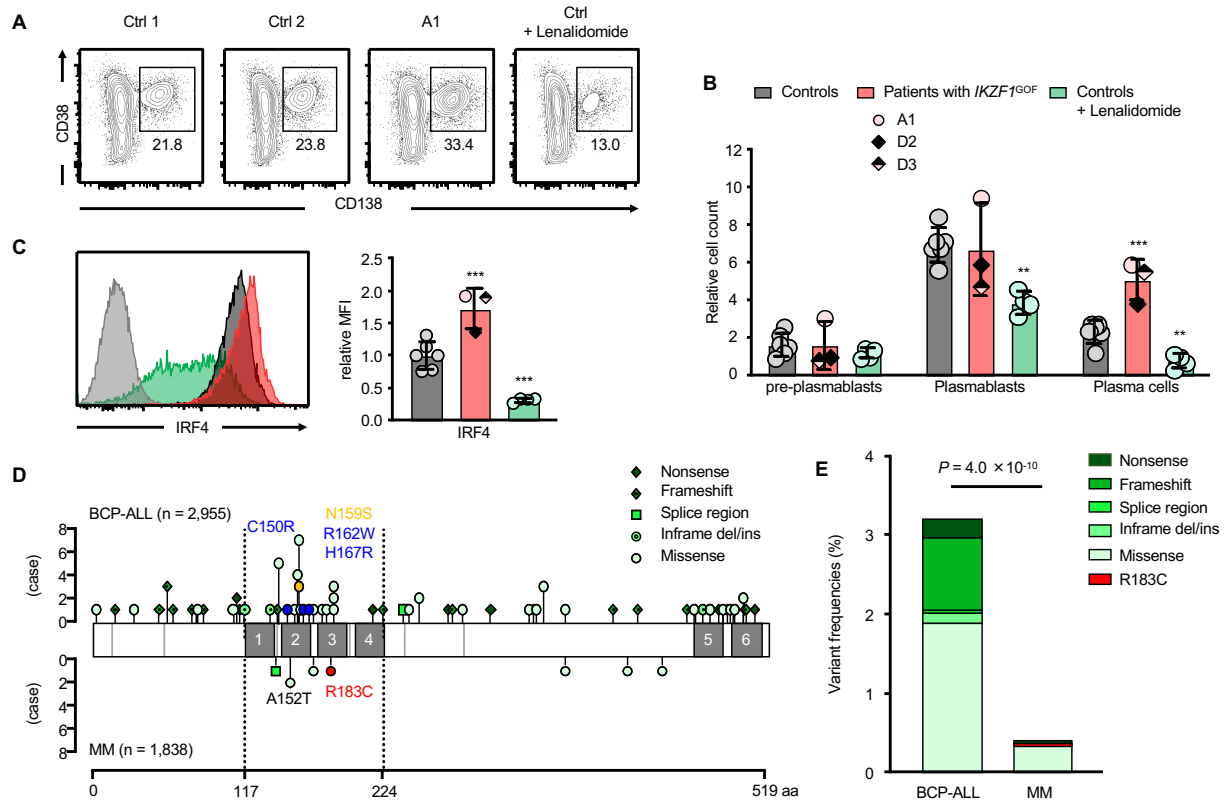
IKZF1^{WT}, IKZF1^{R162Q}, IKZF1^{N159S}, IKZF1^{R183H} or IKZF1^{R183C}, or empty vector, and mCherry⁺ cells were sorted 3 days after infection. Cells were cultured in anti-CD3 mAb-coated plates for 7 days in the presence or absence of lenalidomide (10 μM). **(A)** Expression of IKZF1 by western-blot from lysates of mCherry⁺ cells. KU80 was used as loading control. **(B)** Graphs of frequencies of IL-2 (left panel), IFN-γ (middle panel) or IL-4 (right panel) positive cells that were re-stimulated with PMA plus ionomycin for 6 h (IL-2) or overnight (IFN-γ or IL-4) and analyzed by intracellular staining. Data from FACS analyses. **(C)** Same as in (B) excepted that the mRNA expression of *TBX21* was analyzed by qPCR. Data normalized on *GAPDH* mRNA expression. In (B) and (C), bars are presented as mean ± SD from four independent experiments with one in which addition of lenalidomide was not tested. Comparison between groups were analyzed with one-way ANOVA with Holm-Šidák multiple-comparisons test. *P < 0.05, **P < 0.01, ***P < 0.001.

Fig. 5. Reduced Treg and increased Tfh in *IKZF1*^{GOF} patients



(A) FACS analyses of gated CD4⁺ T cells showing naïve Treg (CD45RA⁺FOXP3^{low}), effector Treg (CD45RA⁻FOXP3^{high}) and non-Treg/Tfr (CD45RA⁻FOXP3^{low}) from PBMCs of controls (Ctrl), one *IKZF1*^{HI} (R143W) patient, one *IKZF1*^{DN} (N159T) patient and *IKZF1*^{GOF} (A1, B1, B2, B3, C1, D1 and D2) patients. Dot plots (upper panels) and graphs of the frequencies in CD4⁺ T cells (lower panel) from FACS analyses. **(B)** Analysis of *in vitro* Treg differentiation of CD4⁺CD45RA⁺CCR7⁺CD25⁻ T cells from controls and one *IKZF1*^{GOF} (A1) patient cultured with anti-CD3 mAb-coated plate, anti-CD28 mAb and TGF-β1 in the presence or absence of IL-2 for 6 days. Graphs from FACS analyses showing frequencies of FOXP3⁺ cells. **(C)** Graphs of frequencies of CD45RA⁻CXCR5⁺ Tfh gated on CD4⁺ T cells (left panel) and CD45RA⁻FOXP3⁺ Tfr gated on Tfh cells (right panel) from FACS analyses of PBMCs of patients. In (B) data from two independent experiments including one in which the patient was tested with three controls. In (A) to (C), bars are presented as mean ± SD. Comparison between groups were analyzed with Mann-Whitney *U* test in (A) and one-way ANOVA with Holm-Šidák multiple-comparisons test in (C). **P* < 0.05, ****P* < 0.001.

Fig. 6. Increased generation of plasma cells (PCs) and multiple myeloma associated with *IKZF1*^{GOF}



(A) PC differentiation of CD19⁺CD27⁺ memory B cells from controls (Ctrl) or *IKZF1*^{GOF} patients (A1, D2 and D3) in the presence or absence of lenalidomide. FACS analyses of gated CD20⁻ cells showing CD38⁺CD138⁺ plasma cells. Numbers correspond to percentage of CD38⁺CD138⁺ cells in the gates. **(B)** Relative counts of pre-plasmablasts (CD20⁻CD38⁻CD138⁻), plasmablasts (CD20⁻CD38⁺CD138⁻) or PCs (CD20⁻CD38⁺CD138⁺) from controls, *IKZF1*^{GOF} patients or controls with lenalidomide at day 10. Relative counts of memory B cells at day 0 defined as 1. **(C)** Histograms from FACS analyses of intracellular IRF4 expression in PCs at day 10. Isotype control in gray and graphs showing MFI of IRF4 (right panel). **(D)** IKZF1 structure showing the somatic variants found in BCP-ALL (top) and MM (bottom). Variants corresponding to *IKZF1*^{HI}, *IKZF1*^{DN} or *IKZF1*^{GOF} are in blue, yellow and red, respectively. **(E)** Frequencies of somatic *IKZF1* variants in B-cell precursor acute lymphoblastic leukemia (BCP-ALL) and multiple myeloma (MM). Bars as mean ± SD. In (C) and (B), data from two independent experiments. Comparison between groups analyzed with one-way ANOVA with Dunnett's post hoc multiple-comparisons test in (B) and (C), or chi-square test in (E). **P < 0.01, ***P < 0.001.

Table 1. Clinical manifestations of patients with *IKZF1*^{R183H/C} variants

| Patient (variant) | Age at first presentation/evaluation (years) | Origin | Autoimmunity/inflammation (autoantibodies) | Atopy/allergy | Plasma cell proliferation | Other manifestations | Treatment |
|-------------------|--|--------------------------|--|--|--|---|---------------------------------------|
| A1 (R183H) | 2/17 | Caucasian (North Africa) | ES, celiac disease (ANA, ASMA, tTG-IgA) | asthma, rhinitis | no | no | rituximab, gluten free diet |
| B1 (R183H) | 47/49 | Caucasian (Turkey) | non-typed DM (ANA, ASMA) | no | lymphadenopathy | pseudotumor cerebri | rituximab, sirolimus, steroids |
| B2 (R183H) | 16/18 | Caucasian (Turkey) | ES, type 1 DM, autoimmune hepatitis, Hashimoto thyroiditis, leucoclastic vasculitis (direct Coombs, ANA, ASMA, P-ANCA, anti-TPO, anti-TG, tTG-IgA, anti-gliadin IgG) | no | lymphadenopathy | no | rituximab sirolimus |
| B3 (R183H) | asymptomatic/16 | Caucasian (Turkey) | no (no) | no | no | no | ND |
| C1 (R183H) | 22/26 | Caucasian (US) | ES, colitis, bowel perforation (ND) | no | lymphadenopathy, infiltration in intestine and bile duct | aortic regurgitation, otitis media, plantar warts, acne | steroids |
| D1 (R183C) | 1/39 | Caucasian (US) | alopecia, vitiligo, colitis (no) | dermatitis, asthma, rhinitis, eosinophilic esophagitis, drug allergy | polyclonal proliferation in BM | sinopulmonary bacterial infections | colectomy, tofacitinib, steroid, HSCT |
| D2 (R183C) | 2/41 | Caucasian (US) | no (no) | dermatitis, asthma, rhinitis, food allergy | no | sinus and ear infections | IVIG |
| D3 (R183C) | 0.5/11 | Caucasian (US) | alopecia (no) | dermatitis, asthma, rhinitis, food allergy | no | otitis media | IVIG |

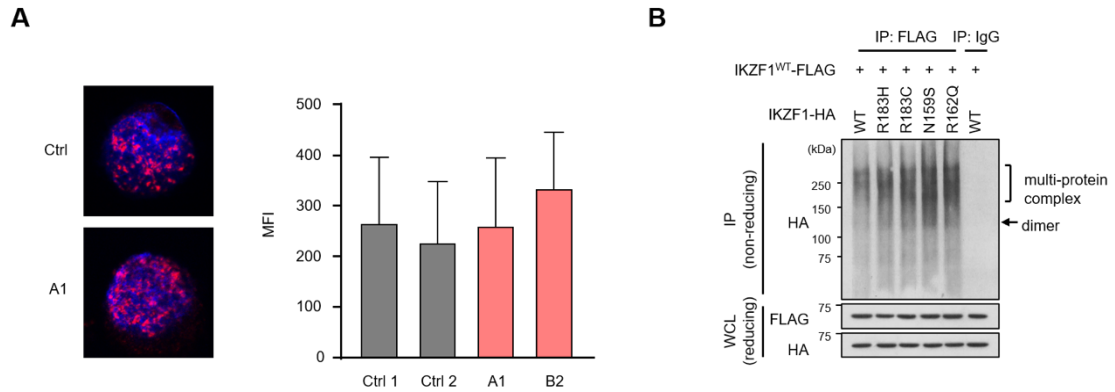
ANA, antinuclear antibody; anti-TG, anti-thyroglobulin antibody; anti-TPO, anti-thyroperoxidase antibody; ASMA, anti-smooth muscle antibody; BM, bone marrow; DM, diabetes mellitus; ES, Evans syndrome; ND, not determined; HSCT, hematopoietic stem cell transplantation; IVIG, intravenous immunoglobulin; P-ANCA, perinuclear anti-neutrophil cytoplasmic antibody; tTG-IgA, anti-tissue transglutaminase IgA antibody.

20

21

22 **Supplementary Figure S2. Subcellular localization and dimerization**

23



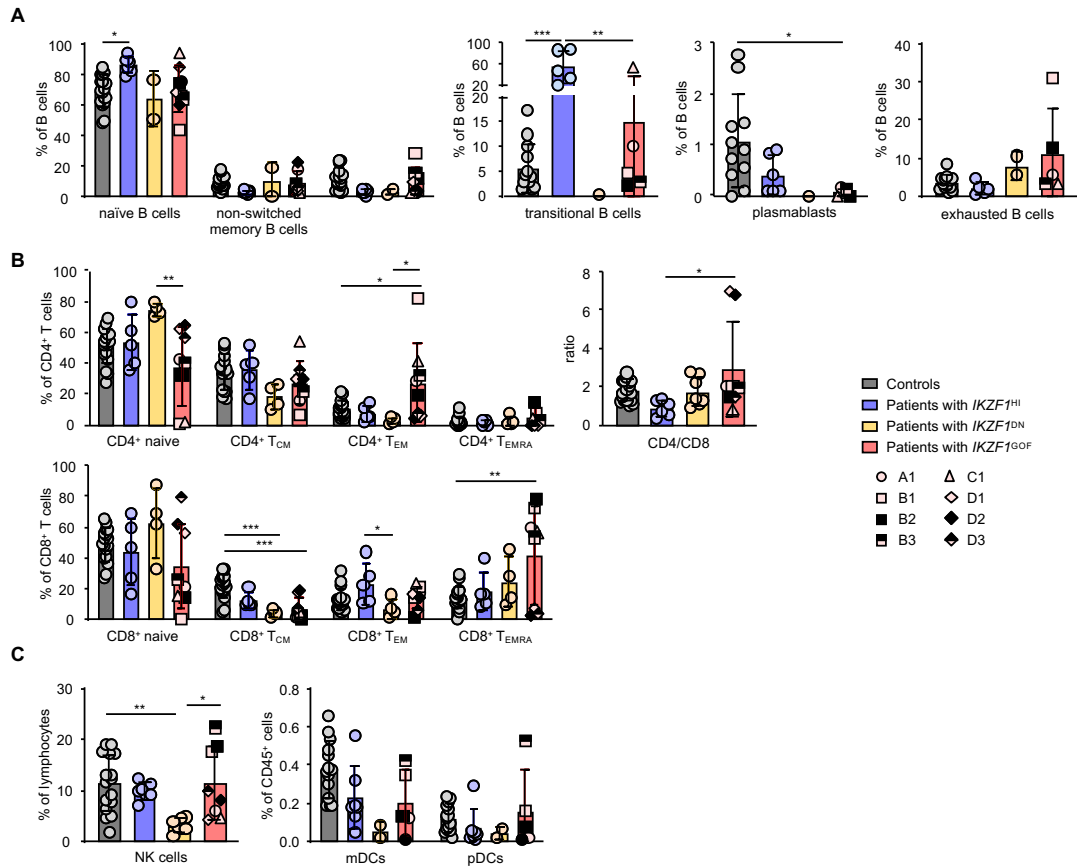
24

25 **(A)** The localization of IKZF1 in T cells from patients A1, B2 and controls that were
26 stimulated with anti-CD3/CD28-coated beads for 24 h. Cells were incubated with anti-
27 IKZF1 rabbit antibody followed by Alexa Fluor 488-conjugated anti-rabbit antibody (red)
28 and DAPI (blue) (left panel). Graph shows mean fluorescence intensity (MFI) of Alexa
29 Fluor 488 (right panel.) **(B)** Co-immunoprecipitation (IP) of FLAG-tagged WT IKZF1
30 and HA-tagged WT IKZF1 or HA-tagged IKZF1 mutants (R183C, R183H, N159S and
31 R162Q) with anti-FLAG mouse antibody from lysates of HEK-293T cells that were
32 transiently co-transfected with the corresponding vectors. Mouse IgG isotype matched
33 (IgG) was used as a negative control. IP samples were immunoblotted with anti-HA
34 antibody in non-reducing condition (upper panel). Whole cell lysates (WCL) were
35 immunoblotted with anti-FLAG (middle panel) or anti-HA (lower panel) antibodies in
36 reducing conditions.

37

38

39 **Supplementary Figure S3. Immune phenotyping of PBMCs.**



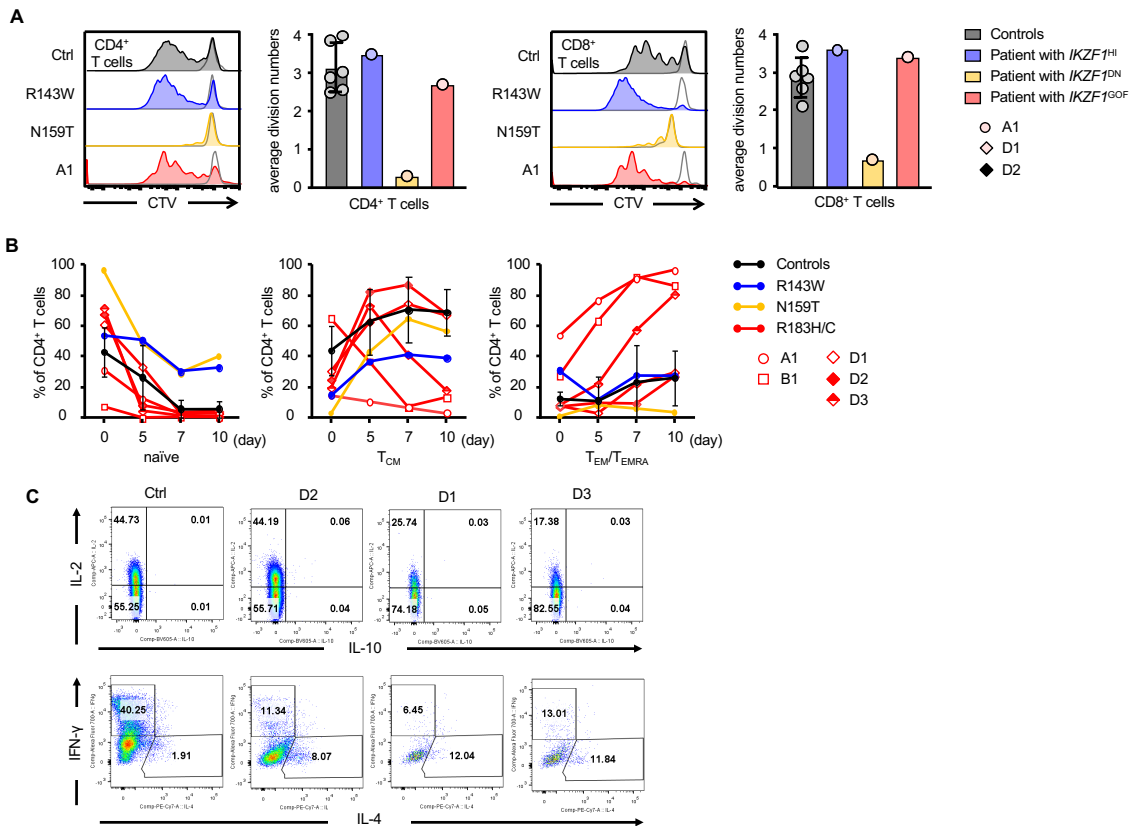
40

41 **(A)** Graph bars showing relative proportions of B-cell phenotype; naïve (IgD⁺CD27⁻),
 42 non-switched memory (IgD⁺CD27⁺), switched memory (IgD⁻CD27⁺), transitional
 43 (IgM⁺CD38⁺) B cells, plasmablasts (IgM⁻CD38⁺), and exhausted (CD21⁻CD38⁻) B cells.
 44 **(B)** CD4/CD8 ratio and T-cell phenotype; naïve (CD45RA⁺CCR7⁺), central memory
 45 (T_{CM}; CD45RA⁻CCR7⁺), effector memory (T_{EM}; CD45RA⁻CCR7⁻) and terminally
 46 differentiated effector memory (T_{EMRA}; CD45RA⁺CCR7⁻) T cells. **(C)** Relative
 47 proportions of NK cells and myeloid/plasmacytoid DCs in PBMCs. In (A-C), *IKZF1*^{HI}
 48 (C147R, R162Q and R162W), *IKZF1*^{DN} (N159S/T) and *IKZF1*^{GOF} (R183H/C) patients
 49 were tested several times. Data from FACS analyses. Data are presented as mean ± SD.
 50 Comparison between groups were analyzed with one-way ANOVA with Holm-Šidák
 51 multiple-comparisons test. *P < 0.05, **P < 0.01, ***P < 0.001.

52

53

54 **Supplementary Figure S4. Proliferation, differentiation and cytokine productions of**
 55 **T cells.**



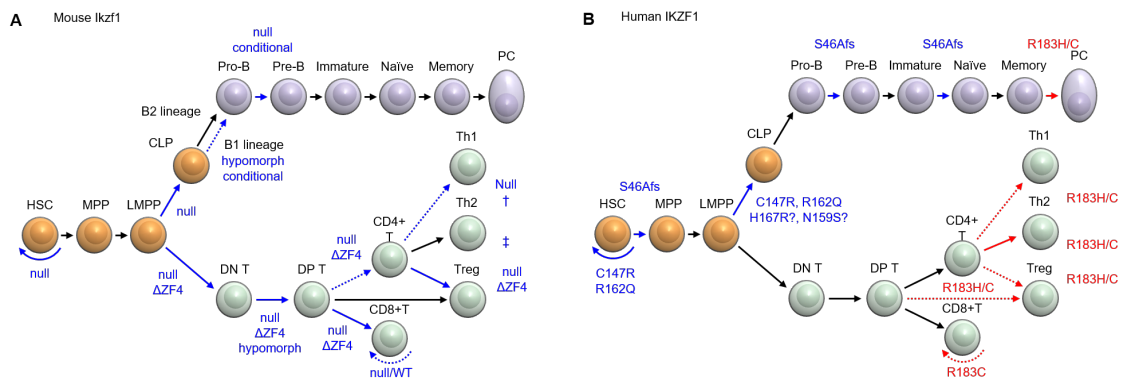
56

57 **(A)** Proliferation of CD4⁺ (left panels) and CD8⁺ (right panels) T cells of controls,
 58 *IKZF1*^{HI} (R143W), *IKZF1*^{DN} (N159T) and *IKZF1*^{GOF} (A1) patients determined by
 59 dilution of cell trace violet (CTV) dye analyzed by flow cytometry at day 3 after
 60 stimulation with anti-CD3 mAb-coated plates. **(B)** PBMCs of controls, *IKZF1*^{HI}
 61 (R143W), *IKZF1*^{DN} (N159T) and *IKZF1*^{GOF} (A1, B1, D1, D2 and D3) patients were
 62 cultured with PHA for 3 days and then with IL-2. Frequencies of naïve
 63 (CD45RA⁺CCR7⁺), central memory (T_{CM}; CD45RA⁻CCR7⁺), effector memory (T_{EM};
 64 CD45RA⁻CCR7⁻) and terminally differentiated effector memory (T_{EMRA};
 65 CD45RA⁺CCR7⁻) CD4⁺ T cells were obtained from FACS analyses at day 0, 5, 7 and
 66 10. **(C)** FACS analyses of IL-2, IL-10, IFN-γ and IL-4 intracellular production gated on
 67 CD4⁺ T cells from PBMCs of one control (Ctrl) and *IKZF1*^{GOF} (D2, D1 and D3) patients
 68 stimulated with PMA plus ionomycin for 6 h.

69

70

71 **Supplementary Figure S5. Schematic diagram of IKZF1 roles in T/B-cell**
72 **development.**



73

74 **(A)** Role of mouse *Ikzf1* based on studies of the different mice models deficient for *ikzf1*
75 (references 2-5). The steps impaired in these different deficient models are shown by blue
76 arrows **(B)** Role human IKZF1 based on studies of different variants. Bone marrow cells
77 were previously examined in 5 *IKZF1*^{HI} patients (C147R, R162Q, R167R and
78 S46Afs*14) (references 8, 9, 38) and 2 *IKZF1*^{DN} patients (N159S) (10). Partial block from
79 pro-B to pre-B cells was observed in one patient with *IKZF1*^{S46Afs*14}, but not in two
80 patients with *IKZF1*^{C147R} or *IKZF1*^{R162Q}. In patients with *IKZF1*^{H167R} and *IKZF1*^{N159S}, pro-
81 B (CD34⁺CD19⁺) and early B-cell precursors (CD34⁺cTdT⁺CD19^{+/-}) were markedly
82 decreased. The steps impaired by loss-of-function variants (*IKZF1*^{HI} and *IKZF1*^{DN}) are
83 shown by blue arrows, while those increased by gain-of-function variants (R183C/H)
84 reported here are shown in red arrows. Solid arrows indicate positive regulations, while
85 dotted arrows indicate negative regulations (by wild-type *ikzf1* or IKZF1).

86 † In CD4⁺ specific conditional null mice, increased IFN- γ expression was observed in
87 Th2 polarizing conditions but not in Th1 polarizing conditions.

88 ‡ Although involvement was suggested by *Ikzf1*^{null} mice, CD4⁺ specific conditional null
89 mice did not display a defect in *Gata3* or IL-4 expression.

90 Δ ZF4, deletion of ZF4; hypomorph, LacZ insertion into exon 2; HSC, hematopoietic
91 stem cell; MPP, multipotent progenitor; LMPP, lymphoid-primed multi-potent
92 progenitors; CLP common lymphoid progenitor; DN, CD4⁻CD8⁻ double negative; DP,
93 CD4⁺CD8⁺ double positive.

94

95 **Supplementary Table S1.**

96 **Total and specific immunoglobulin levels and post vaccination serologies**

| Patient | C1 | Normal values |
|--------------------------------------|----------------|---------------|
| Immunoglobulin levels | | |
| IgG1 (mg/dL) | 1,315 | 351-962 |
| IgG2 (mg/dL) | 440 | 239-838 |
| IgG3 (mg/dL) | >220 | 8.5-140 |
| IgG4 (mg/dL) | 555.9 | 4.5-117 |
| Specific IgG antibodies | | |
| <i>Streptococcus pneumoniae</i> | Positive 1/23* | |
| <i>Haemophilus influenzae</i> type b | Negative | |
| Tetanus | Positive | |
| Diphtheria | Positive | |
| Mumps | Negative | |
| Rubella | Positive | |
| Measles | Positive | |

97 * Positive for serotype 20. Negative for serotypes 1, 2, 3, 4, 5, 6B, 7F, 8, 9N, 9V, 10A, 11A, 12F, 14,

98 15B, 17F, 18C, 19A, 19F, 22F, 23F and 33F.

99

100 **Supplementary Table S2. Immunological features of peripheral blood from**
 101 **patients with *IKZF1*^{R183H/C} variants**

| Patient | A1 | B1 | B2 | B3 | C1 | D1 | D2 | D3 | |
|--|-------|-------|-------|-------|-------|--------|--------|-------|---------------|
| Gender | M | F | F | M | M | F | M | M | |
| Age at evaluation | 17 | 49 | 18 | 16 | 26 | 41 | 42 | 13 | Normal values |
| Leukocytes (cells/mm ³) | 7,200 | 8,800 | 9,500 | 6,400 | 5,820 | 12,440 | 5,520 | 2,630 | 3,980-10,040 |
| Neutrophils (%) | 40 | 71 | 56 | 47 | 82.1 | 78 | 50 | 72 | 34.0-71.1 |
| Lymphocytes (%) | 44 | 11 | 26 | 33 | 5.8 | 14 | 30.8 | 15.5 | 19.3-51.7 |
| Monocytes (%) | 9 | 11 | 5 | 9 | 8.4 | 5.5 | 8.2 | 7 | 4.7-12.5 |
| Eosinophils (%) | 7 | 6 | 13 | 11 | 2.7 | 1.6 | 10.3 | 3 | 0.7-5.8 |
| Basophils (%) | <1 | <1 | <1 | <1 | 0.3 | 0.3 | 0.5 | 0.5 | 0.1-1.2 |
| Erythrocytes (× 10 ⁴ cells/mm ³) | 518 | 472 | 542 | 529 | 520 | 367 | 477 | 441 | 393-522 |
| Hemoglobin (g/dL) | 15.2 | 13.7 | 15.5 | 16.3 | 14.1 | 12.5 | 15.1 | 13.0 | 11.2-15.7 |
| Hematocrit (%) | 42.4 | 47.2 | 45.8 | 45.6 | 45.6 | 38.5 | 45.8 | 40.6 | 34.1-44.9 |
| Platelets (× 10 ⁴ cells/mm ³) | 6.8 | 23.9 | 25.6 | 18.4 | 21.0 | 48.0 | 22.1 | 40.1 | 17.3-36.9 |
| T-cell lineages (%) | | | | | | | | | |
| T cells (CD3 ⁺ /Lymphocytes) | 75.0 | 73.3 | 70.2 | 62.4 | 89.9 | 95.0 | 87.8 | 83.4 | 62.4-87.2 |
| Helper T cells (CD4 ⁺ /CD3 ⁺) | 64.0 | 55.7 | 45.8 | 59.7 | 26.7 | 86.4 | 83.7 | 56.5 | 50.0-69.8 |
| Helper T, naive (CD45RA ⁺ CCR7 ⁺ /CD3 ⁺ CD4 ⁺) | 42.6 | 0.6 | 32.1 | 40.6 | 1.9 | 63.5 | 65.7 | 57.5 | 16.2-80.2 |
| Helper T, T _{CM} (CD45RA ⁻ CCR7 ⁺ /CD3 ⁺ CD4 ⁺) | 15.8 | 6.3 | 28.4 | 22.2 | 53.9 | 30.2 | 29.7 | 35.9 | 22.1-65.3 |
| Helper T, T _{EM} (CD45RA ⁻ CCR7 ⁻ /CD3 ⁺ CD4 ⁺) | 28.5 | 83.0 | 18.9 | 32.2 | 41.2 | 6.1 | 4.6 | 6.6 | 4.9-33.2 |
| Helper T, T _{EMRA} (CD45RA ⁺ CCR7 ⁻ /CD3 ⁺ CD4 ⁺) | 13.1 | 8.4 | 14.5 | 2.5 | 3.0 | 0.1 | 0.0 | 0.0 | 0.0-3.2 |
| Cytotoxic T cells (CD8 ⁺ /CD3 ⁺) | 32.0 | 27.6 | 31.3 | 30.0 | 31.7 | 12.3 | 12.2 | 37.1 | 24.4-42.8 |
| Cytotoxic T, naive (CD45RA ⁺ CCR7 ⁺ /CD3 ⁺ CD8 ⁺) | 22.1 | 0.9 | 14.3 | 26.7 | 15.8 | 57.3 | 63.0 | 80.1 | 24.8-85.5 |
| Cytotoxic T, T _{CM} (CD45RA ⁻ CCR7 ⁺ /CD3 ⁺ CD8 ⁺) | 1.1 | 3.0 | 1.1 | 2.3 | 4.1 | 17.9 | 19.4 | 7.8 | 6.5-44.8 |
| Cytotoxic T, T _{EM} (CD45RA ⁻ CCR7 ⁻ /CD3 ⁺ CD8 ⁺) | 16.6 | 21.1 | 2.2 | 13.5 | 23.0 | 17.1 | 14.8 | 6.5 | 4.8-40.0 |
| Cytotoxic T, T _{EMRA} (CD45RA ⁺ CCR7 ⁻ /CD3 ⁺ CD8 ⁺) | 60.2 | 73.6 | 79.5 | 54.0 | 57.1 | 7.7 | 2.8 | 4.9 | 3.0-33.9 |
| Recent thymic emigrants (CD31 ⁺ CD45RA ⁺ /CD3 ⁺ CD4 ⁺) | 42.3 | 2.9 | 24.9 | 19.3 | 1.9 | ND | ND | ND | 29.5-63.4 |
| Follicular helper T cells (CD45RO ⁺ CXCR5 ⁺ /CD3 ⁺ CD4 ⁺) | 25.7 | 9.1 | 26.6 | 14.0 | 1.9 | 4.1 | 5.8 | ND | 1.7-10.5 |
| B-cell lineages (%) | | | | | | | | | |
| B cells (CD19 ⁺ /Lymphocytes) | 21.0 | 3.2 | 5.1 | 12.3 | 5.9 | 0.5 | 4.5 | 6.4 | 6.1-18.7 |
| Naive B cells (CD27 ⁻ /CD19 ⁺) | 75.3 | 43.9 | 74.5 | 64.6 | 94.9 | 68.4 | 60.2 | 85.6 | 43.3-91.5 |
| Non-switched memory B cells (CD27 ⁺ IgD ⁺ /CD19 ⁺) | 18.1 | 3.8 | 3.2 | 8.3 | 1.7 | 3.6 | 22.6 | 6.1 | 2.7-20.2 |
| Switched memory B cells (CD27 ⁺ IgD ⁻ /CD19 ⁺) | 2.2 | 27.9 | 11.2 | 15.0 | 1.7 | 9.1 | 3.5 | 4.1 | 3.3-30.1 |
| NK-cell lineage (%) | | | | | | | | | |
| NK cells (CD16 ⁺ CD56 ⁺ /Lymphocytes) | 6.0 | 17.8 | 18.6 | 22.4 | 4.5 | 4.3 | 8.0 | 9.9 | 1.3-17.5 |
| Dendritic-cell lineages (%) | | | | | | | | | |
| Myeloid DCs (HLA-DR ⁺ CD11c ⁺ CD123 ⁻ /CD45 ⁺) | 0.12 | 0.35 | 0.13 | 0.42 | 0.01 | ND | ND | ND | 0.13-0.93 |
| Plasmacytoid DCs (HLA-DR ⁺ CD11c ⁻ CD123 ⁺ /CD45 ⁺) | 0.02 | 0.16 | 0.08 | 0.53 | 0.01 | ND | ND | ND | 0.03-0.70 |
| Immunoglobulin levels | | | | | | | | | |
| IgG (mg/dL) | 1,273 | 2,484 | 2,200 | ND | 2,466 | 1,041 | 820 | 613 | 700-1,600 |
| IgA (mg/dL) | 263 | 936 | 346 | ND | 288 | 1,543 | 252 | 226 | 70-400 |
| IgM (mg/dL) | 128 | 125 | 186 | ND | 227 | 24 | 80 | 30 | 40-230 |
| IgE (IU/mL) | 746.0 | ND | ND | ND | 2,459 | 36.9 | 2135.0 | 695.0 | <173 |

102 Red and blue numbers blue indicate values above and below the normal range respectively compared to age-matched controls.

103

104

106 **Supplementary Table S3. *IKZF1* somatic variants in BCP-ALL or MM**

| Disease | Cohort | Patient ID | <i>IKZF1</i> variant |
|---------|-------------------|--------------|----------------------|
| BCP-ALL | AYA_CALGB | SJBALL021878 | V57fs, G158S |
| BCP-ALL | AYA_CALGB | SJBALL021835 | F486fs |
| BCP-ALL | AYA_ECOG | SJBALL020139 | E76fs |
| BCP-ALL | AYA_ECOG | SJBALL020163 | N159Y |
| BCP-ALL | AYA_ECOG | SJBALL020134 | N159fs |
| BCP-ALL | AYA_ECOG | SJBALL020096 | D186G |
| BCP-ALL | AYA_ECOG | SJBALL020161 | V239fs |
| BCP-ALL | AYA_ECOG | SJBALL020121 | C464W |
| BCP-ALL | AYA_ECOG | SJBALL020071 | R502W |
| BCP-ALL | AYA_MDACC | SJBALL021702 | P113fs |
| BCP-ALL | AYA_MDACC | SJBALL021743 | D186A |
| BCP-ALL | AYA_MDACC | SJBALL021718 | K307* |
| BCP-ALL | AYA_MDACC | SJBALL021719 | G496S |
| BCP-ALL | COG | SJBALL021479 | M31V |
| BCP-ALL | COG | SJBALL020555 | R51Gfs |
| BCP-ALL | COG | SJBALL020366 | D81N |
| BCP-ALL | COG | SJBALL021541 | G108V |
| BCP-ALL | COG | SJBALL020738 | R111* |
| BCP-ALL | COG | SJBALL021344 | L117fs |
| BCP-ALL | COG | SJBALL020385 | R137Efs |
| BCP-ALL | COG | SJBALL020473 | Q156H |
| BCP-ALL | COG | SJBALL020568 | G158S |
| BCP-ALL | COG | SJBALL021312 | G158S |
| BCP-ALL | COG | SJBALL020602 | N159Y |
| BCP-ALL | COG | SJBALL020623 | N159Y |
| BCP-ALL | COG | SJBALL020655 | N159Y |
| BCP-ALL | COG | SJBALL020607 | D186A |
| BCP-ALL | COG | SJBALL020899 | D186Y |
| BCP-ALL | COG | SJBALL021317 | H224fs |
| BCP-ALL | COG | SJBALL020667 | G337S |
| BCP-ALL | COG | SJBALL020779 | V340Pfs |
| BCP-ALL | COG | SJBALL020453 | Y348C |
| BCP-ALL | COG | SJBALL020673 | Y348C |
| BCP-ALL | COG | SJBALL020676 | Y348C |
| BCP-ALL | COG | SJBALL021352 | S402fs |
| BCP-ALL | COG | SJBALL020367 | M476T |
| BCP-ALL | COG | SJBALL020811 | M476delinsPR |
| BCP-ALL | COG_AYA_Dedicated | SJBALL020952 | V57fs |
| BCP-ALL | COG_AYA_Dedicated | SJBALL021125 | V57fs |
| BCP-ALL | COG_AYA_Dedicated | SJBALL021118 | Q62fs |
| BCP-ALL | COG_AYA_Dedicated | SJBALL021076 | R143Q |
| BCP-ALL | COG_AYA_Dedicated | SJBALL021094 | H167R |
| BCP-ALL | COG_AYA_Dedicated | SJBALL020984 | D252N |
| BCP-ALL | COG_AYA_Dedicated | SJBALL021004 | P342L |
| BCP-ALL | COG_AYA_Dedicated | SJBALL020991 | A365V |
| BCP-ALL | COG_AYA_Dedicated | SJBALL020963 | F471delinsLRA |
| BCP-ALL | COG_AYA_Dedicated | SJBALL021089 | R487C |
| BCP-ALL | COG_AYA_Dedicated | SJBALL021067 | C492W |
| BCP-ALL | COG_AYA_Dedicated | SJBALL021058 | R502W |
| BCP-ALL | COG_AYA_Leg | SJBALL262 | L85_G94fs, Y180N |
| BCP-ALL | COG_AYA_Leg | SJBALL021371 | R111* |
| BCP-ALL | COG_AYA_Leg | SJBALL021346 | V239_E6splice_region |
| BCP-ALL | COG_AYA_Leg | SJBALL020563 | D252N |

| | | | |
|---------|-------------|----------------|------------------|
| BCP-ALL | COG_AYA_Leg | SJBALL268 | C495Y |
| BCP-ALL | COG_AYA_Leg | SJBALL021443 | E504fs |
| BCP-ALL | St Jude | SJBALL085 | E80fs |
| BCP-ALL | St Jude | SJBALL011 | R162P |
| BCP-ALL | St Jude | SJBALL095 | S277fs |
| BCP-ALL | Li et al. | ND | D2Y |
| BCP-ALL | Li et al. | ND | S17fs |
| BCP-ALL | Li et al. | ND | L117_K118insNQ |
| BCP-ALL | Li et al. | ND | R137_S138insAL |
| BCP-ALL | Li et al. | ND | R143Q |
| BCP-ALL | Li et al. | ND | R143Q |
| BCP-ALL | Li et al. | ND | R143Q |
| BCP-ALL | Li et al. | ND | G158S |
| BCP-ALL | Li et al. | ND | N159Y |
| BCP-ALL | Li et al. | ND | N159Y |
| BCP-ALL | Li et al. | ND | N159Y |
| BCP-ALL | Li et al. | ND | E170K |
| BCP-ALL | Li et al. | ND | D186A |
| BCP-ALL | Li et al. | ND | D186G |
| BCP-ALL | Li et al. | ND | L216X |
| BCP-ALL | Li et al. | ND | T244A |
| BCP-ALL | Li et al. | ND | D285N |
| BCP-ALL | Li et al. | ND | M459fs |
| BCP-ALL | Li et al. | ND | Y503X |
| BCP-ALL | Li et al. | ND | R511X |
| BCP-ALL | Lana et al. | DCOG-6 | G142Pfs, p.R144Q |
| BCP-ALL | Lana et al. | AIEOP-28 | C150R |
| BCP-ALL | Lana et al. | EORTC-9 | N159S |
| BCP-ALL | Lana et al. | MRC-UK-12 | N159S |
| BCP-ALL | Lana et al. | BFM-G-13 | N159S |
| BCP-ALL | Lana et al. | MRC-UK-4 | L160V, R274* |
| BCP-ALL | Lana et al. | MRC-UK-13 | R162W |
| BCP-ALL | Lana et al. | BFM-G-22 | D186Tfs |
| BCP-ALL | Lana et al. | BFM-G-1 | H421Pfs |
| BCP-ALL | Lana et al. | EORTC-1 | E465Dfs |
| BCP-ALL | Lana et al. | BFM-G-20 | C483Pfs |
| BCP-ALL | Lana et al. | AIEOP-24 | F490Yfs |
| MM | M3P | 122 | A152T |
| MM | M3P | 540 | A152T |
| MM | M3P | 119 | E170D |
| MM | M3P | 534 | Y413C |
| MM | M3P | 526 | R439H |
| MM | MMRF | MMRF_1725_1_BM | S364L |
| MM | MMRF | MMRF2787 | c.421+2T>A |
| MM | Lohr et al. | ND | R183C |

107 See References 40-43

